HYDRONAUTICS, incorporated
research in hydrodynamics

THE LINEARIZED THEORY FOR SUPERCAVITATING HYDROFOILS OPERATING AT HIGH SPEEDS NEAR A FREE SURFACE

by

J. Auslaender

8 June 1961

HYDRONAUTICS, Incorporated

TABLE OF CONTENTS

HYDRONAUTICS, Incorporated

ABSTRACT

Linearized cavity flow theory, in conjunction with a mapping technique, is used to develop general expressions for the characteristics of super-cavitating or fully ventilated, two dimensional hydrofoils with prescribed pressure distributions, designed for operation near a free surface. It is assumed that the hydrofoils are operating at zero cavitation number and that the Froude number - based on depth - is very large. The general expressions are used to derive the lift, cavity drag and shape of hydrofoils composed of 2-, 3-, and 5-term and constant pressure camber configurations, combined with angle of attack and quasi-parabolic thickness and designed for operation at specific depths. Examples of numerical results are given and the effect of foil strength is discussed and evaluated.

NOTATION

A, a	Constants in the conformal transformation, depending on depth
C_D	Drag Coefficient $= \dfrac{D}{\frac{1}{2}\rho U_\infty^2 \, c}$
C_L	Lift Coefficient $= \dfrac{L}{\frac{1}{2}\rho U_\infty^2 \, c}$
C_M	Moment Coefficient $= \dfrac{M}{\frac{1}{2}\rho \, U_\infty^2 \, c^2}$
c	Chord length
$C_D(h, k_i, \delta, \tau)$	Drag Coefficient of a foil designed for depth-chord ratio h, with camber distribution type i, camber index k_i, design angle of attack δ and quasi-parabolic thickness coefficient τ
$C_L(h, k_i, \delta)$	Lift Coefficient of a foil designed for depth-chord ratio h, with camber distribution type i, camber index k_i, and design angle of attack δ
$C_M(h, k_i, \delta)$	Moment Coefficient of a foil designed for depth-chord ratio h, with camber distribution type i, camber index k_i, and design angle of attack δ
D	Two dimensional cavity drag
h	Depth of submersion / chord
k_i	Camber index of camber distribution type i. i takes on the values 1, 2, 3 or 5 to denote that the camber distribution is of the constant pressure, two-term, three-term or five-term type, respectively
L	Two dimensional lift on the hydrofoil
M	Two dimensional moment about the leading edge of the hydrofoil, positive in the direction tending to pitch the nose up

HYDRONAUTICS, Incorporated

-iii-

p	Local pressure on the bottom surface of the hydrofoil
p_c	Cavity pressure
p_∞	Static pressure in the free stream
Δp	Pressure difference between the upper and lower surfaces of the hydrofoil
S	Leading edge suction force on a fully wetted airfoil, positive in the direction of U_∞
u	The x component of the perturbation velocity in the hydrofoil plane, expressed as a fraction of U_∞
$\bar{u}$	The x component of the perturbation velocity in the airfoil plane, expressed as a fraction of U_∞
v	The y component of the perturbation velocity in the hydrofoil plane, expressed as a fraction of U_∞
$\bar{v}$	The y component of the perturbation velocity in the airfoil plane, expressed as a fraction of U_∞
x	A space coordinate in the hydrofoil plane, parallel to U_∞; its origin coincides with the leading edge of the foil. Distance along the chord of the hydrofoil expressed as a fraction of chord length
y	Vertical space coordinate in the hydrofoil plane, expressed as a fraction of the chord length
y_o	Ordinate of the bottom surface of the hydrofoil expressed as a fraction of the chord length
y_c	Ordinate of the top cavity boundary, expressed as a fraction of the chord length
Z	Hydrofoil section modulus
$\bar{Z}$	Non-dimensional section modulus $= Z/c^3$
z	A complex variable $= x + i\, y$
γ	Vortex strength
δ	Design angle of attack of the hydrofoil
ζ	A complex variable $= \xi + i\, \eta$

η Imaginary coordinate in the airfoil plane

θ A dummy variable in the airfoil plane, defined by $\xi = \frac{1}{2}(1-\cos\theta)$

ξ Real coordinate in the airfoil plane

ξ' A dummy variable along the ξ axis

ρ Mass density of incompressible fluid

σ Cavitation number $= (p_\infty - p_c) / \frac{1}{2}\rho U_\infty^2$

τ Quasi-parabolic thickness coefficient

The quantities $\overline{A}$, $\overline{B}$, $\overline{C}$, $\overline{D}$, $\overline{E}$, $\overline{F}$, $\overline{G}$, $\overline{H}$, $\overline{J}$, $\overline{K}$, $\overline{L}$, $\overline{M}$, G', H', J', K', L', M', R, Q and b are defined on pages 18 -19

L_2 Dilogarithm, defined on page 23

The quantities $\overline{P}$ and $\overline{Q}$ are defined on page 22

HYDRONAUTICS, Incorporated

LIST OF FIGURES

HYDRONAUTICS, Incorporated

Figure Number

HYDRONAUTICS, Incorporated

THE LINEARIZED THEORY FOR SUPERCAVITATING HYDROFOILS
OPERATING AT HIGH SPEEDS NEAR A FREE SURFACE

INTRODUCTION

Increasing interest in the design of high speed hydrofoil craft has made it necessary to review some of the basic contributions in the field of supercavitating or ventilated lifting surfaces and to investigate the effect of the proximity of a free surface on their design. The exact solution of the problem of a supercavitating inclined flat plate near a free surface was obtained by Green (1)[*] and was necessarily given in terms of the spray thickness rather than the depth of submersion. This solution was discussed by Johnson (2) who presented it in practicable form together with experimental relationships between the spray thickness and the depth of submersion. It is evident, however, that in view of the large cavitation drag on a flat plate at both finite and infinite depths, it is of great importance to specify low drag (i.e., cambered) hydrofoil sections.

Tulin and Burkart (3) first showed that the problem of the supercavitating hydrofoil could be converted into the problem of a thin airfoil whose lower surface pressures are positive or zero and that, for reasons of hydrodynamic efficiency, the center of pressure of the foil should be as close to the trailing edge as possible. They introduced a low drag supercavitating camber configuration by specifying the pressure distribution on the equivalent airfoil as the first two terms of a trigonometric series and optimizing its coefficients, and proceeded to calculate the characteristics of specific

---

[*]Numbers in parenthesis refer to the list of References.

hydrofoils, designed for operation at infinite depth, by combining
that camber configuration with angle of attack. Anticipating a
possible increase in hydrodynamic efficiency, Johnson (4) intro-
duced camber configurations derived from pressure distributions de-
fined by the first three and the first five terms of a trigonometric
series whose coefficients are also optimized so as to give zero or
positive pressures on the lower surface and a center of pressure
as far aft as possible. Hydrofoils incorporating these types of
camber configuration have since come to be known as Two-, Three-
and Five-Term Foils and are very useful in infinite depth applica-
tions. Specifically, two-term foils are being used in the design
of supercavitating propellers (5).

If a hydrofoil designed for infinite depth is to be operated
at a finite depth the necessity for maintaining the condition of
shock free entry (i.e. the dividing streamline coincides with the
leading edge) requires that the foil be operated at an angle of
attack which is smaller than the original (infinite depth) design
angle. The lift and the chordwise pressure distribution due to
camber also change as the depth of submersion is varied. An approxi-
mate method for calculating the effect of depth on angle of attack
and on the lift due to camber has been given by Johnson (6) who
also performed experiments which corroborated the theoretical pre-
dictions almost completely.

Johnson resorted to an approximation because of the very
complicated integrals which arise in applying even the linear theory
to the problem of determining the finite depth characteristics of
a supercavitating hydrofoil of specified shape. The results he
obtained are adequate and very useful in ascertaining the effect
of depth variation on the performance of a given foil. It is pos-
sible, however, to design hydrofoils for specified, finite depths
without having to resort to approximations to the linear theory.

This is done by specifying the pressure distribution that is to result at the esired operating depth, rather than specifying the shape of the hydrofoil. This approach results in hydrofoils which are designed for specific depths and deliver hydrodynamic performance that is somewhat superior to that of foils designed for infinite depth but operating at finite depth. In the present work the linearized theory (3) is used to derive general expressions, in terms of an arbitrary pressure distribution, for the shape and performance characteristics of any supercavitating ($\sigma=0$) hydrofoil designed for any specified depth. In addition to the limitations of linear theory the only conditions attached to the validity of these expressions is that the pressures be positive over the entire bottom surface of the foil, that the cavity begin at the leading edge and that the cavitation number based on cavity pressure be zero.

The general expressions are used to calculate the lower surface shape, cavity shape, lift and drag of two-, three- and five-term hydrofoils and of a hydrofoil on which the pressure distribution is constant over the chord. From the results of these calculations and from a consideration of a hypothetical foil on which the pressure distribution is that due to a single vortex it is evident that the hydrodynamic efficiency of a foil depends to a very great extent on the location of its center of pressure. From the point of view of increasing the lift-drag ratio it would be desirable to have the center of pressure as close as possible to the trailing edge. Strength considerations, however, indicate that the center of pressure should be located near the foil leading edge and dictate that the loading at the nose not vanish. The two-, three- and five-term camber configurations, if used by themselves without additional angle of attack, would deliver very high lift-drag ratios but would leave much to be desired from the point of

view of strength. Specifically, the value of L/D for a given lift increases as the center of pressure is moved to the rear, but in all three camber shapes, when the lift is produced by camber alone, the location of the upper cavity boundary near the leading edge is, according to the linear theory, <u>below</u> the theoretical bottom surface of the foil. The constant pressure distribution results in camber configurations whose strength is somewhat improved but whose lift-drag ratios are relatively poor.

The first remedy that suggests itself is the standard one of combining the various camber distributions with angle of attack. The high leading edge pressures associated with angle of attack have the effect -- at the cost of reduced lift-drag ratios -- of greatly enlarging the cavity thickness and hence (since the foil can be thickened to fill the entire cavity without affecting its hydro-dynamic characteristics) result in increased strength. The lin-earized characteristics of a flat plate operating near a free sur-face are calculated by using Munk's inversion formula (7) to derive the pressure distribution and incorporating it into the above men-tioned general expressions for lift, drag and upper cavity shape.

In addition, the strength characteristics can be improved -- at moderate cost in drag -- by superimposing upon the foil the pres-sure distribution generated by a single vortex located at the lead-ing edge of the equivalent airfoil. The bottom shape associated with this leading-edge-concentrated pressure is a semi-parabola in foils designed for infinite depth and a similar, quasi-parabolic configuration in foils designed for finite depths. Thus the pres-sure concentration at the nose has the effect of rounding the otherwise very sharp leading edge in addition to increasing the overall area of the foil section.

It will be shown how the performance characteristics and shapes due to camber (e.g., two-term, three-term, five-term or

constant pressure) are to be combined with those due to angle of attack and quasi-parabolic thickness to obtain the shape and characteristics of a foil composed of a set of these three parameters.

As in the work of Tulin-Burkart (3) and Johnson (4), the method selected for the treatment of the hydrofoil problem is the use of the concept of an equivalent airfoil derived from a suitable conformal transformation.

THE HYDROFOIL-AIRFOIL EQUIVALENCE

In considering the problem of a supercavitating or fully ventilated hydrofoil at a finite depth below a free surface it is assumed that (a) the limitations of linear theory apply (i.e., the velocity perturbations are small in comparison to the forward speed of the foil), and (b) the cavitation number σ is zero. Asumptions (a) and (b) are the same as those used in the design of infinite depth hydrofoils. In addition it is postulated that (c) the Froude number based on depth is very large so that on the free surface the velocity perturbation in the x direction (the direction of the stream) is zero.

With these assumptions, the problem of the thin hydrofoil near a free surface, schematically illustrated in Figure 1, can be represented by a semi-infinite slit on the x axis in the complex $z = x + iy$ plane, the free surface being represented by the line $y = h$. This configuration, shown in Figure 2 together with the relevant boundary conditions, is a simply connected polygon B_∞, C_∞, C'_∞, D, E, B_∞ which lends itself to a Schwarz Christoffel transformation of the type

$$\frac{dz}{d\zeta} = \frac{A\zeta}{\zeta + a} \tag{1}$$

where $z = x + iy$ is the complex space coordinate in the hydrofoil
plane,

$\zeta = \xi + i\eta$ is the complex space coordinate in the airfoil
plane, and

A and a are constants depending on the depth/chord ratio h. This transformation maps the entire z plane into the lower half of the ζ plane.

With the above mentioned boundary conditions and the constraints that

when $x = 0$ $\xi = 0$

and when $x = 1$ $\xi = 1$, *

the integration of the transformation [1] and its separation into the real and imaginary parts yield the result

$$x + i0 = aA[\frac{\xi}{a} - \ln(1 + \frac{\xi}{a})] \text{ where } \xi < 0$$

$$x - i0 = aA[\frac{\xi}{a} - \ln(1 + \frac{\xi}{a})] \text{ where } \xi > 0$$

[2]

where

$$aA\pi = h$$

[3a]

and

$$\frac{1}{A} = 1 - \ln \frac{1+a}{a} .$$

[3b]

Plots of a and A vs. depth-chord ratio and of $\frac{x}{aA}$ vs. $\frac{\xi}{a}$ are shown in Figures 3 and 4.

As shown in Figure 2 and indicated in equation [2], the upper half of the z plane maps into the negative ξ axis and the lower half of the z plane maps into the positive ξ axis. Thus the abcissa of a point (x, y_c) on the upper cavity streamline in the z plane is represented by a <u>negative</u> ξ in the ζ plane and the abcissa of a point (x, y_o) on the lower cavity streamline (i.e., the lower surface of the foil and the lower boundary of the trailing cavity) is represented by a positive ξ in the ζ plane. Equations [3a] and [3b] together

---

*All distances are normalized with respect to the chord length of the hydrofoil and all perturbation velocities are normalized with respect to the speed of the stream at infinity, U_∞.

constitute an implicit solution for a and A in terms of the depth-chord ratio h.

At the limits of zero and infinite depth the asymptotic values of the constants and the transformation are:

$$\text{when } h \to 0 \quad \begin{cases} a \to 0 \\ A \to 1 \\ x-10 \to \xi \text{ where } \xi > 0 \end{cases} \qquad [4]$$

Note that on the surface (h = 0) there is no distortion between the airfoil and the hydrofoil.

$$\text{when } h \to \infty \quad \begin{cases} a \to \infty \\ A \to 2a \\ x+10 \to \xi^2 \text{ where } \xi < 0 \\ x-10 \to \xi^2 \text{ where } \xi > 0 \end{cases} \qquad [5]$$

Thus, at infinite depth the transformation [2] reduces to the one used by Tulin and Burkart (3).

LIFT, DRAG, MOMENT AND CAVITY SHAPE

The lift on the hydrofoil and the moment about its leading edge may be written as

$$L = \int_0^1 \Delta p \, dx \qquad [6]$$

and

$$M = - \int_0^1 \Delta p x \, dx \qquad [7]$$

(positive in the direction tending to pitch the nose up) where Δp = the pressure difference between the face and back of the hydrofoil.

Using the linearized Bernoulli equation

$$p + \rho U_\infty^2 u = p_\infty \tag{8}$$

where

ρ = the mass density of the fluid

U_∞ = the velocity very far upstream and downstream of the foil

u = $u(x)$ = the ratio of the perturbation velocity on the lower (pressure) side of the hydrofoil to the free stream velocity U_∞

and p = the pressure on the lower (pressure) side of the foil,

and noting that since the cavitation number is zero the pressure on the upper surface of a supercavitating foil is p_∞, we get

$$\Delta p = p - p_\infty = -\rho\, U_\infty^2 u \ . \tag{9}$$

In the linearized cavity flow theory lines of constant perturbation velocities remain unchanged when transformed from the z to the ζ plane (and vice versa). Consequently the conformal transformation has no effect on the perturbation velocities u and v, other than to distort the x location at which a given velocity exists (i.e., the pressure--proportional to u--at a point x on the hydrofoil is exactly the same as the pressure at the corresponding point ξ on the airfoil), so that

$$u(x) = \overline{u}\,(\xi) \tag{10}$$

(unbarred quantities refer to the hydrofoil; barred quantities, to its equivalent airfoil).

Combining the real part of equation [1] and equations [2], [9], and [10], and normalizing with respect to $\frac{1}{2}\rho U_\infty^2$ we get, for

the lift and moment coefficients,

$$C_L = -2 \int_0^1 \frac{A\xi}{\xi + a} \bar{u}(\xi)d\xi \qquad [11]$$

and

$$C_M = 2 \int_0^1 x \frac{A\xi}{\xi+a} \bar{u}(\xi)d\xi = 2 \int_0^1 aA[\frac{\xi}{a} - \ln(1+ \frac{\xi}{a})]\frac{A\xi}{\xi+a} \bar{u}(\xi)d\xi \quad . \quad [12]$$

In the limits of h = 0 and h = ∞ these expressions reduce to

$$C_L = -2 \int_0^1 \bar{u}(\xi)d\xi \qquad (h=0) \qquad [11a]$$

$$C_L = -2 \int_0^1 2\xi\bar{u}(\xi)d\xi \qquad (h=\infty) \qquad [11b]$$

and

$$C_M = 2 \int_0^1 \xi\bar{u}(\xi)d\xi \qquad (h=0) \qquad [12a]$$

$$C_M = 2 \int_0^1 2\xi^3\bar{u}(\xi)d\xi \qquad (h=\infty) \qquad . \qquad [12b]$$

In linear theory, the drag on an element of chord of a hydrofoil may be expressed as the product of the lift on and the slope $\frac{dy_0}{dx}$ of that element. Using the linearized boundary conditions (shown in Figure 2) and the fact that angles (e.g., $\frac{dy}{dx}$) are not affected by the transformation, we may write

$$\frac{dy}{dx} = v(x) = \bar{v}(\xi) \qquad [13]$$

where $v(x)U_\infty$ = the perturbation velocity in the y direction on the bottom of the hydrofoil,

and $\bar{v}(\xi)U_\infty$ = the perturbation velocity in the η direction on the positive ξ axis in the airfoil plane.

Hence the drag

$$D = \int_0^1 \bar{v}(\xi)\Delta p dx = -\rho U_\infty^2 \int_0^1 \bar{v}(\xi)\bar{u}(\xi) \frac{A\xi}{\xi+a} d\xi \quad . \qquad [14]$$

As shown by Tulin and Burkart (3), $\bar{v}(\xi)$ can be expressed in terms of $\bar{u}(\xi)$ in the following manner: The downwash at a point ξ on the hydrofoil, induced by a vortex of strength γ, located at ξ' is $\frac{\gamma}{2\pi(\xi'-\xi)}$. Since $\gamma = -2\bar{u}(\xi')$, (negative because $\bar{u}(\xi')$ is the velocity perturbation on the <u>bottom</u> of the hydrofoil), the downwash, integrated over the chord, becomes

$$\frac{dy_o}{dx} = \bar{v}(\xi) = \frac{1}{\pi} \int_0^1 \frac{\bar{u}(\xi')}{\xi-\xi'} d\xi' \quad \text{where} \quad 0 \le \xi \le 1 \qquad [15]$$

Combining equations [14] and [15] and normalizing we get

$$C_D = 2 \int_0^1 \int_0^1 - \frac{A}{\pi} \left[\frac{\bar{u}(\xi)\bar{u}(\xi')\xi}{(\xi+a)(\xi-\xi')} \right] d\xi d\xi'$$

$$= 2 \int_0^1 \int_0^1 - \frac{A}{\pi}(\frac{1}{2})\left[\frac{\xi}{(\xi+a)(\xi-\xi')} + \frac{\xi'}{(\xi'+a)(\xi'-\xi)} \right] \bar{u}(\xi)\bar{u}(\xi') d\xi d\xi'$$

$$= \frac{Aa\pi}{\pi^2} \int_0^1 \int_0^1 - \left[\frac{\bar{u}(\xi)}{\xi+a} \right]\left[\frac{\bar{u}(\xi')}{\xi'+a} \right] d\xi d\xi' \qquad (a \ne 0)$$

and finally, using equation [3a],

$$C_D = \frac{h}{\pi^2} \left[\int_0^1 - \frac{\bar{u}(\xi)}{\xi+a} d\xi \right]^2 \qquad (a \ne 0) \qquad [16]$$

In the limiting case of infinite depth the drag coefficient becomes

$$C_D = \frac{2}{\pi} \left[\int_0^1 \bar{u}(\xi) d\xi \right]^2 \qquad (h=\infty) \qquad [16a]$$

At zero depth the hydrofoil becomes a planing surface and its cavity drag is, in all respects, synonymous with the <u>spray drag</u> experienced by such surfaces. Wagner (8) long ago showed that, except in the immediate neighborhood of the leading edge, the high speed flow past a planing surface was identical to the flow past

the lower surface of an identically formed fully wetted airfoil.
The difference between the two flows (in the immediate neighbor-
hood of the leading edge) consists in the fact that the leading
edge suction force experienced by a fully wetted airfoil does not
exist on a planing surface (or, for that matter, on any super-
cavitating hydrofoil) and is replaced -- on the planing surface
only -- by spray. Wagner showed that the total drag on a planing
surface was equal to half the drag on the identical fully wetted
airfoil less half the leading edge suction force S acting on the
latter. Since the total drag on a fully wetted airfoil in an in-
viscid fluid is zero, the spray drag can be written as

$$D = - \tfrac{1}{2} S \qquad (h = 0)$$

The magnitude of the leading edge suction force S is well known
in airfoil theory and is given by Jones (9) as

$$S = \lim_{x \to 0} - \pi \rho U_\infty^2 \left[u(x) \sqrt{x} \right]^2$$

Combining the last two equations, normalizing with respect to
$\tfrac{1}{2}\rho U_\infty^2$ and noting that at h=0, x=ξ we get, for the spray drag co-
efficient

$$C_D = \lim_{x \to 0} \pi \left[\bar{u}(\xi) \sqrt{\xi} \right]^2 \qquad (h=0) \qquad\qquad [16b]$$

Equation [16b] shows that if the pressure (proportional to
u) on the lower surface, at the leading edge of the foil goes to
infinity as $\sqrt{\xi}$ -- the flat plate is a case in point -- the spray
drag is indeed a finite quantity. It also shows, as Wagner (8)
anticipated, that by proper use of camber it is possible to produce
lift without spray or spray drag. It will be seen below that the
two-term, three-term, five-term and constant pressure camber con-
figurations fulfill this ambition.

The ordinates of the lower and upper cavity streamlines

$(y_0$ and y_c respectively) are obtained by integrating their slopes.
The slope of the lower cavity boundary (i.e., the bottom surface
of the foil) has already been given in equation [15]. Employing
the same reasoning but keeping in mind that the upper part of the
hydrofoil is mapped into the <u>negative</u> ξ axis, the slope of the upper
cavity streamline can be shown to be[*]

$$\frac{dy_c}{dx} = \overline{v}(-\xi) = \frac{1}{\pi} \int_0^1 \frac{\overline{u}(\xi')}{\xi - \xi'} \, d\xi' \quad \text{where} \quad -\infty \leq \xi \leq 0 \quad [17]$$

and the ordinates of the upper cavity boundary of the hydrofoil and
lower surface are

$$y_c(\xi) = \int_0^\xi \overline{v}(-\xi') \frac{A\xi'}{\xi' + a} \, d\xi' \quad \text{where} \quad -a < \xi \leq 0 \quad [18]$$

and

$$y_0(\xi) = \int_0^\xi \overline{v}(\xi') \frac{A\xi'}{\xi' + a} \, d\xi' \quad \text{where} \quad 0 \leq \xi \leq 1 \quad [19]$$

Note that [18] and [19] give the cavity ordinates in the hydro-
foil plane in terms of abcissas in the airfoil plane. This is only
due to the fact that the transformation (equation [2]) cannot be
inverted to give an explicit expression for ξ in terms of x, and
can be remedied in the process of plotting the actual cavity shapes.

In the limiting cases of zero and infinite depth the upper
and lower cavity ordinates become

---

[*]It is pointed out that in spite of the similarity of the integrands
in equations [15] and [17] the expressions (after integrations) for
$\overline{v}(-\xi)$ and $\overline{v}(\xi)$ will be entirely dissimilar due to the fact that
equation [15] contains a singular integral.

$$y_o(x) = \int_0^x \overline{v}(\xi') \, d\xi' \qquad (h = 0)$$

$$\left. \begin{array}{l} y_c(x) = \int_0^{-\sqrt{x}} 2\,\overline{v}(\xi') \, \xi' d\xi' \\[12pt] y_o(x) = \int_0^{\sqrt{x}} 2\,\overline{v}(\xi') \, \xi' d\xi' \end{array} \right\} \qquad (h = \infty) \qquad [20]$$

In equations [11], [12], [16], [18], and [19] we have the means to calculate the lift, moment, drag and upper and lower cavity ordinates of a supercavitating hydrofoil, designed for any specified depth, in terms of the $\overline{u}$ perturbation velocity (and hence, the pressure) on the bottom of its equivalent airfoil. The conditions relevant to the validity of these equations are that (a) a cavity does indeed exist everywhere on the upper hydrofoil surface, (b) there is no cavitation anywhere on the lower surface, (c) the linear theory holds, (d) the cavitation number is zero, and (e) the Froude Number is very large.

It is often convenient to express the pressures on a given hydrofoil as the sum of a number of different types of pressure distributions. Conversely, analysis of the characteristics of various types of pressure distribution often leads to the conclusion that it might be advisable to combine some of them into one foil. Such a foil is referred to as a composite foil whose various components are the shapes associated with each of the specific types of pressure distribution. Each of the characteristics of the composite foil is a function of all its component pressure distributions in addition to being a function of depth. Denoting n different component pressure distributions by u_1, u_2, $\ldots$, u_n, the characteristics of a composite foil are found from equations

[11], [12], [16], [18] and [19]:

$$C_L(h,u_1, u_2, \ldots, u_n) = C_L(h,u_1 0, \ldots, 0) + C_L(h, 0, u_2, \ldots 0)$$

$$+ \ldots + C_L(h, 0, 0, \ldots, u_n) \qquad [21]$$

$$C_M(h, u, u_2, \ldots, u_n) - C_M(h, u_1, 0, \ldots 0) + C_M(h, 0, u_2, \ldots, 0)$$

$$+ \ldots C_M(h, 0, 0, \ldots u_n) \qquad [22]$$

$$C_D(h, u_1, u_2, \ldots, u_n) = (\sqrt{C_D(h, u_1, 0, \ldots, 0)} + \sqrt{C_D(h, 0, u_2, \ldots, 0)}$$

$$+ \ldots + \sqrt{C_D(h, 0, 0, \ldots u_n)} \;)^2 \qquad [23]$$

$$y_0(h, x, u_1, u_2, \ldots, u_n) = y_0(h, x, u_1, 0, \ldots, 0) + y_0(h, x, 0, u_2, \ldots, u_n)$$

$$+ \ldots + y_0(h, x, 0, 0, \ldots, u_n) \qquad [24]$$

and

$$y_c(h, x, u_1, u_2, \ldots, u_n) = y_c(h, x, u_1, 0, \ldots, 0) + y_c(h, x, 0, u_2, \ldots, 0)$$

$$+ \ldots + y_c(h, x, 0, 0, \ldots, u_n) \qquad [25]$$

Notation of the type $C_L(h, u_1, u_2, \ldots, u_n)$, introduced here in general terms, will be used later to denote the characteristics of depth-adapted hydrofoils which are combinations of camber (denoted by k_1), angle of attack δ and quasi-parabolic thickness τ. The types of camber configurations that will be considered are the constant pressure (k_1), the two-term (k_2), the three-term (k_3) and the five-term (k_5). Thus, for example, $y_0(h, x, k_3, \delta, \tau)$ denotes

the bottom surface ordinate, at x, of a three-term foil which has been designed for operation at a depth of h chords and whose camber index, angle of attack and thickness coefficient have the values k_3, δ and τ, respectively; $C_L(1,0,2.5^o)$ is the lift coefficient developed by a flat plate operating at a depth of 1 chord at an angle of attack of 2.5 degrees; and $C_D(1,0,2.5^o,0.01)$ is the drag coefficient of a quasi-parabolic shape designed for operation at a depth of one chord with a thickness coefficient of 1% at an angle of attack of 2.5 degrees.

The general expressions will now be used to calculate the lift, drag, moment and shape of depth adapted camber configurations which are characterized by certain specified types of pressure distributions.

THE OPTIMUM PRESSURE DISTRIBUTION

Tulin and Burkart (3) have shown that for the class of all possible cavitating hydrofoils the absolute optimum pressure distribution is that in which the pressure is entirely concentrated at the trailing edge of the foil. They pointed out that in spite of the fact that such a pressure distribution cannot be realized on any practical hydrofoil the performance of this "optimum foil" is a very convenient criterion against which the lift-drag efficiency of all other supercavitating foils can be measured. The lift-drag ratio of the optimum foil, designed for infinite depth, was shown to be $\dfrac{8\pi}{C_L}$. It is of interest to find the value of this optimum ratio for foils designed for other depths.

Let us consider the pressure distribution in the airfoil plane, shown in Figure 4, which is such that the pressures are entirely concentrated at a point ξ_o. The distribution of the $\overline{u}$ velocity on the bottom surface of the foil can then be expressed as

$$\overline{u}(\xi) = -K\delta(\xi-\xi_o) \qquad [26]$$

where K is a constant and $\delta(\xi-\xi_o)$ is the Dirac delta function
which is such that

$$\delta(\xi-\xi_o) = \begin{array}{l} 0 \text{ for } \xi-\xi_o \neq 0 \\ \infty \text{ for } \xi-\xi_o = 0 \end{array}$$

$$\int_{-\infty}^{\infty} \delta(\xi-\xi_o)d\xi = 1$$

and

$$\int_{-\infty}^{\infty} \delta(\xi-\xi_o) \, f(\xi) \, d\xi = f(\xi_o)$$

Combining equation [26] with (N) and [16] we obtain

$$\frac{C_L}{C_D} = \frac{4h}{a^2 C_L} \, \xi_o^2 \qquad [27]$$

Clearly, the largest possible lift-drag ratio will be obtained
when $\xi_o = 1$ (i.e., the pressures are concentrated at the trailing
edge) so that

$$\left(\frac{L}{D}\right)_{opt} = \frac{4h}{a^2 C_L}$$

Figure 5 illustrates how the optimum lift-drag ratio for a given
lift coefficient varies with depth. As can be seen, $\left(\frac{L}{D}\right)_{opt}$ for a
depth of one chord is almost four times as high as that for infinite
depth. Equation [27] also illustrates that in the absence of
strength requirements (which, in a practical case, might be over-
whelming) the center of pressure should be located as far aft as
possible.

HYDRONAUTICS, Incorporated

THE TWO-, THREE- AND FIVE-TERM CAMBER DISTRIBUTIONS

The perturbation velocity in the airfoil plane on the two-term camber distribution is given by Tulin and Burkart (3) as

$$\bar{u}(\xi) = - \frac{8}{5\pi} k_2 (\sin\theta - \tfrac{1}{2} \sin 2\theta) \tag{28}$$

where θ is a dummy variable defined by

$$\xi = \tfrac{1}{2}(1 - \cos\theta)$$

Johnson (4) showed that for the three-term camber

$$\bar{u}(\xi) = - \frac{4}{3\pi} k_3 (\sin\theta - \sin 2\theta + \tfrac{1}{2} \sin 3\theta) \tag{29}$$

and for the five-term camber

$$\bar{u}(\xi) = - \frac{6}{5\pi} k_5 (\sin\theta - \frac{4}{3} \sin 2\theta + \frac{4}{3} \sin 3\theta - \frac{2}{3} \sin 4\theta$$

$$+ \frac{1}{3} \sin 5\theta) \tag{30}$$

the $\bar{u}$ distributions for given values of k_2, k_3, and k_5 are shown in Figure 6. The coefficients k_2, k_3, and k_5 serve the purpose of scaling the magnitude of the respective pressure distributions and, hence, serve also as scaling factors for the C_L, C_M, C_D and shape of the three types of camber configuration. These coefficients shall be termed the 2-, 3- and 5-term camber index. It will be seen that for camber configurations designed for infinite depth the numerical value of the camber index is also equal to the value of the lift coefficient when no angle of attack is present.

When the expressions for $\bar{u}(\xi)$ given in equations [28], [29] and [30] are combined with equations [11], [16], [18], and [19] the following expressions for the lift, drag, bottom shape and top cavity shape of the three camber configurations are obtained:[*]

---

[*] The work involved is one of straightforward, if sometimes laborious, integrations demanding special care when improper integrals are indicated. For some of the more complicated integrations the tables of integrals in [10] and [11] were used.

First, let

$$\overline{A} = \xi - a \ln \frac{a+\xi}{a} = \frac{a\pi}{h} x$$

$$\overline{B} = \tfrac{1}{2}\xi^2 - a\overline{A}$$

$$\overline{C} = \frac{1}{3} \xi^3 - a\overline{B}$$

$$\overline{D} = \tfrac{1}{4} \xi^4 - a\overline{C}$$

$$\overline{E} = \frac{1}{5} \xi^5 - a\overline{D}$$

$$\overline{F} = \frac{1}{6} \xi^6 - a\overline{E}$$

$$R = \sqrt{\xi^2 - \xi} \quad \text{for } (\xi < 0)$$

$$\overline{G} = \tfrac{1}{2} (\xi - \tfrac{1}{2}) R - \tfrac{1}{8} \ln (1-2\xi-2R)$$

$$\overline{H} = \frac{1}{3} R^3 + \tfrac{1}{2} \overline{G}$$

$$\overline{J} = \tfrac{1}{4} \xi R^3 + \frac{5}{8} \overline{H}$$

$$\overline{K} = \frac{1}{5} \xi^2 R^3 + \frac{7}{10} \overline{J}$$

$$\overline{L} = \tfrac{1}{6}\xi^3 R^3 + \frac{3}{4} \overline{K}$$

$$\overline{M} = R - (a+\tfrac{1}{2})\ln(1-2\xi-2R) - \sqrt{a^2+a} \ \ln \ \frac{a-(2a+1)\xi+2 \sqrt{a^2+a} \ R}{a + \xi}$$

where ξ is defined by equation [2],

$$\text{let } Q = \sqrt{x + \sqrt{x}}$$

$$G' = -\tfrac{1}{2} (\sqrt{x} + \tfrac{1}{2}) Q - \tfrac{1}{8} \ln (1 + 2\sqrt{x} - 2Q)$$

$$H' = \frac{1}{3} Q^3 + \tfrac{1}{2} G'$$

$$J' = -\tfrac{1}{4} \sqrt{x} \ Q^3 + \frac{5}{8} H'$$

$$K' = \frac{1}{5} x \ Q^3 + \frac{7}{10} J'$$

$$L' = -\frac{1}{6} x^{3/2} Q^3 + \frac{3}{4} K'$$

$$M' = \frac{1}{7} x^2 Q^3 + \frac{11}{14} L'$$

and let $b = 2a + 2\sqrt{a(1+a)} + 1$.

Then, for the two-term camber:

$$C_L(h,k_2,0) = \begin{cases} \dfrac{4}{5} k_2 & (h = 0) \\[3mm] \dfrac{4hk_2}{5a\pi}\left[1 + 8a^2 (\sqrt{a} - \sqrt{1+a})^2 - 2a\right] & (0 < h < \infty) \\[3mm] k_2 & (h = \infty) \end{cases}$$

$$C_D(h,k_2,0,0) = \begin{cases} 0 & (h = 0) \\[3mm] h\left(\dfrac{4k_2}{5\pi}\right)^2 \left[1 - 4a (\sqrt{a} - \sqrt{1+a})^2\right]^2 & (0 < h < \infty) \\[3mm] \dfrac{8}{25\pi} k_2^2 & (h = \infty) \end{cases}$$

$$y_o(h,x,k_2,0,0) = \begin{cases} \dfrac{4k_2}{5\pi} (x + 2x^2 - \dfrac{8}{3} x^3) & (h = 0) \\[3mm] \dfrac{4hk_2}{5\pi^2}\left[(1-4a-8a^2)(\dfrac{\xi}{a} - \ln \dfrac{a+\xi}{a}) \right. \\[2mm] \qquad \left. + 2a(\dfrac{\xi}{a})^2(1+2a - \dfrac{4}{3} \xi)\right] & (0 < h < \infty) \\[3mm] \dfrac{4k_2}{5\pi} (x + \dfrac{8}{3} x^{3/2} - 4 x^2) & (h = \infty) \end{cases}$$

where ξ is defined by equation [2]

HYDRONAUTICS, Incorporated

$$y_c(h,x,k_2,0,0) = \begin{cases} \dfrac{8hk_2}{5a\pi^2} (\tfrac{1}{2}\overline{A} + 2\overline{B} - 4\overline{C} - 4\overline{H} + 4a\overline{G} - 4a^2\overline{M}) & (0 < h < \infty) \\[4mm] \dfrac{8k_2}{5\pi} (\tfrac{1}{2}x - \dfrac{4}{3}x^{3/2} - 2x^2 - 8 J') & (h = \infty) \end{cases}$$

For the three-term camber:

$$C_L(h,k_3,0) = \begin{cases} \dfrac{2}{3} k_3 & (h = 0) \\[4mm] \dfrac{2hk_3}{3a\pi}\left[1 - \dfrac{4a}{b}\left(1 - \dfrac{1}{b} + \dfrac{1}{2b^2}\right)\right] & (0 < h < \infty) \\[4mm] k_3 & (h = \infty) \end{cases}$$

$$C_D(h,k_3,0,0) = \begin{cases} 0 & (h = 0) \\[4mm] h\left(\dfrac{4k_3}{3b\pi}\right)^2\left(1 - \dfrac{1}{b} + \dfrac{1}{2b^2}\right)^2 & (0 < h < \infty) \\[4mm] \dfrac{2}{9\pi} k_3^2 & (h = \infty) \end{cases}$$

$$y_o(h,x,k_3,0,0) = \begin{cases} \dfrac{2k_3}{3\pi}(x - 3x^2 + \dfrac{32}{3}x^3 - 8 x^4) & (h = 0) \\[4mm] \dfrac{4hk_3}{3a\pi^2}(\tfrac{1}{2}\overline{A} - 3\overline{B} + 16\overline{C} - 16\overline{D}) & (0 < h < \infty) \\[4mm] \dfrac{2k_3}{15\pi}(5x - 20 x^{3/2} + 80 x^2 - 64 x^{5/2}) & (h = \infty) \end{cases}$$

$$y_c(h,x,k_3,0,0) = \begin{cases} \dfrac{2hk_3}{3a\pi^2}\left[\overline{A}-6\overline{B}+32(\overline{C}-\overline{D}-\overline{J}) + (32a+16)\ \widetilde{H} \right. \\ \qquad\qquad \left. + (32a^2+16a+2)\ (a\overline{M}-\overline{G})\right] \qquad (0<h<\infty) \\[2em] \dfrac{4k_3}{3\pi}\left[\dfrac{x}{2} + 2x^{3/2}+8x^2+ \dfrac{32}{5}\ x^{5/2}-32K' \right. \\ \qquad\qquad\qquad \left. + 16J'-2H'\right] \qquad\qquad (h=\infty) \end{cases}$$

For the five-term camber:

$$C_L(h,k_5,0) = \begin{cases} \dfrac{3}{5}\ k_5 & (h=0) \\[1.5em] \dfrac{3hk_5}{5a\pi}\left[1- \dfrac{4a}{3b}\left(3- \dfrac{4}{b} + \dfrac{4}{b^2} - \dfrac{2}{b^3} + \dfrac{1}{b^4}\right)\right] & (0<h<\infty) \\[1.5em] k_5 & (h=\infty) \end{cases}$$

$$C_D(h,k_5,0,0) = \begin{cases} 0 & (h=0) \\[1.5em] h\left(\dfrac{2k_5}{5b\pi}\right)^2 \left(3- \dfrac{4}{b} + \dfrac{4}{b^2} - \dfrac{2}{b^3} + \dfrac{1}{b^4}\right)^2 & (0<h<\infty) \\[1.5em] \dfrac{9}{50\pi}\ k_5^2 & (h=\infty) \end{cases}$$

$$y_o(h,x,k_5,0,0) = \begin{cases} \dfrac{4k_5}{5\pi}\left(x - 8x^2 + 40x^3 - 92x^4 + \dfrac{512}{5}\ x^5 \right. \\ \qquad\qquad\qquad \left. - \dfrac{128}{3}\ x^6\right) & (h=0) \\[2em] \dfrac{hk_5}{5a\pi^2}(4\overline{A}-64\overline{B}+480\overline{C}-1472\overline{D}+2048\overline{E}-1024\overline{F}) & (0<h<\infty) \\[2em] \dfrac{4k_5}{5\pi}\left(x- \dfrac{32}{3}\ x^{3/2}+60x^2- \dfrac{736}{5}\ x^{5/2}+ \dfrac{512}{3}x^3 \right. \\ \qquad\qquad\qquad \left. - \dfrac{512}{7}\ x^{7/2}\right) & (h=\infty) \end{cases}$$

$$y_c(h,x,k_5,0,0)=\begin{cases} \dfrac{8hk_5}{5a\pi^2}\left[\tfrac{1}{2}\,\overline{A} - 8\overline{B} + 60\overline{C} - 184\overline{D} + 256\overline{E} - 128(\overline{F} + \overline{L}) \right. \\ \qquad\qquad + (128a^4+192a^3+104a^2+24a+2)(a\overline{M} - \overline{G}) \\ \qquad\qquad + (128a^3+192a^2+104a+24)\,\overline{H} \\ \qquad\qquad \left. - (128a^2+192a+104)\overline{J}+(128a+192)\overline{K}\right] \qquad (0<h<\infty) \\[2ex] \dfrac{16k_5}{5\pi}\,(\tfrac{1}{4}\,x + \tfrac{8}{3}\,x^{3/2}+15x^2+ \tfrac{184}{5}\,x^{5/2}+ \tfrac{128}{3}\,x^3+ \tfrac{128}{7}\,x^{7/2} \\ \qquad\qquad - 128M'-2H'+24J'-104K'+192L') \qquad\qquad (h = \infty) \end{cases}$$

THE CONSTANT-PRESSURE CAMBER DISTRIBUTION

Since the perturbation velocity u is proportional to the pressure (equation [9]), the $\overline{u}(\xi)$ associated with pressures that are constant over the chord of the hydrofoil (and, hence, the airfoil) may be written

$$\overline{u}(\xi) = \text{constant} = -\tfrac{1}{2}\,k_1^*$$

and is shown in Figure 6. When this $\overline{u}(\xi)$ is combined with equations [11], [16], [18], and [19] the following expressions for lift, drag, bottom shape and top cavity shape are obtained:

$$C_L(h,k_1,0) = k_1 \qquad\qquad (0 \leq h \leq \infty)$$

$$C_L(h,k_1,0,0) =\begin{cases} 0 & (h = 0) \\[1ex] h\,\left(\dfrac{k_1}{2\pi}\,\ln\dfrac{a+1}{a}\right)^2 & (0 < h < \infty) \\[2ex] \dfrac{k_1^2}{2\pi} & (h = \infty) \end{cases}$$

---

* Due to the standard (NACA) practice of referring to a constant-pressure mean line as an "a = 1 mean line" k_1 has been adopted to denote the camber index associated with this type of pressure distribution. The numerical value of k_1 is the same as the value of the lift coefficient developed by this type of camber (without angle of attack) at any depth.

$$\frac{k_1}{2\pi} \left[x \ln x + (1-x) \ln (1-x) \right] \qquad (h = 0)$$

$$y_o(h,x,k_1,0,0)= \quad \frac{k_1 h}{2\pi^2} \left[\frac{\xi}{a} \ln \frac{1-\xi}{\xi} - \frac{1}{a} \ln (1-\xi) + \ln \frac{\xi+a}{a} \ln \sqrt{\frac{a(\xi+a)}{(1+a)^2}} \right.$$

$$\left. + L_2 \left(\frac{\xi+a}{1+a}\right) - L_2 \left(\frac{a}{1+a}\right) + L_2\left(\frac{a}{\xi+a}\right) - \frac{\pi^2}{6} \right] \quad (0<h<\infty)$$

$$\frac{k_1}{2\pi} \left[(x-1) \ln (1-\sqrt{x}) - x \ln \sqrt{x} - \sqrt{x} \right] \qquad (h = \infty)$$

$$\frac{hk_1}{2\pi^2} \left[\frac{\xi}{a} \ln \frac{\xi-1}{\xi} - \frac{1}{a} \ln (1-\xi) - \ln \frac{a+\xi}{a} \ln (1+a) \right.$$

$$\left. + L_2 \left(\frac{\xi+a}{1+a}\right) - L_2 \left(\frac{a}{1+a}\right) - L_2\left(\frac{\xi+a}{a}\right) + \frac{\pi^2}{6} \right] \quad (0<h<\infty)$$

$$y_c(h,x,k_1,0,0)= \quad \frac{k_1}{2\pi} \left[(x-1) \ln (1+\sqrt{x}) - x \ln \sqrt{x} + \sqrt{x} \right] \qquad (h = \infty)$$

where $L_2 (w) = $ dilogarithm of $w = \sum_{n=1}^{\infty} \frac{w^n}{n^2}$ for $\left| w \right| < 1$

$$L_2(1) = \frac{\pi^2}{6}$$

and ξ is defined by equation [2].

Due to the inordinate difficulties involved in integrating equation [12] analytically, the pitching moments were calculated by performing a separate numerical integration for each depth and each type of pressure distribution. This was accomplished through the use of the IBM 1620 digital computer, installed at HYDRONAUTICS, Incorporated.

The variation of lift coefficient, drag coefficient and the

location of the center of pressure ($\frac{C_M}{C_L}$) with depth, for the two-,

three-, and five-term and the constant pressure types of camber are shown in Figures $7(a)$, $7(b)$, and $7(c)$, respectively. As a typical example, the variation of the lift-drag ratio of the two-term camber with lift coefficient, is shown in Figure 8. The bottom and top cavity shapes of the four types of camber distribution, for depth-chord ratios of 1 and infinity are shown in Figures $9(a)$ and $9(b)$, respectively. Except in the case of the constant pressure type of camber distribution, the upper cavity boundary y_c is seen to lie below y_o, the lower - or pressure - surface of the foil. This result, which implies a crossing of the streamlines, is not attributed to inadequacies of the linear theory. The same phenomenon occurs in many cases in which body shapes are derived, as is done here, from prescribed pressure distributions, regardless of whether the problem is treated with linear or exact theory (see (12) and (13) for discussions of this subject in the literature). The prescribed pressure distribution, which is the starting point of the foil design, immediately implies a theoretical foil shape but the theory, be it linear or exact, which is used to calculate that shape, does not necessarily guarantee it to be physically feasible. The theory does, in fact, penalize us for using overly efficient camber distributions (see Figure 8) by compelling us to accept the reductions in lift-drag ratio that occur when angle of attack and/or quasi-parabolic thickness are combined with camber in order to make the foil a practical possibility and provide it with sufficient strength.

QUASI-PARABOLIC THICKNESS

A vortex of strength $\gamma = \pi \tau U_\infty$ located at the leading edge of the equivalent airfoil will generate a pressure concentrated entirely at the leading edge of the hydrofoil so that the associated $\overline{u}$ velocity distribution may be written in terms of the Dirac-delta function (equation [26]) as

$$\overline{u}(\xi) = -\frac{\pi}{2} \tau \, \delta(\xi)$$

Combining $\overline{u}(\xi)$ with equations [11], [16], [18], and [19] yields the following expressions for the lift, drag, moment and shape associated with the leading-edge-concentrated pressure:

$$C_L \text{ due to } \tau = 0 \qquad (0 < h \leq \infty)$$

$$C_M \text{ due to } \tau = 0 \qquad (0 \leq h \leq \infty)$$

$$C_D(h,0,0,\tau) = \begin{cases} h\left(\dfrac{\tau}{2a}\right)^2 & (0 < h < \infty) \\[2mm] \dfrac{\pi}{2}\tau^2 & (h = \infty) \end{cases}$$

$$\frac{L}{D}(0,0,0,\tau) = 0 \qquad (h = 0)$$

$$y_0(h,x,0,0,\tau) = \begin{cases} -\tau \dfrac{h}{2\pi a} \ln \dfrac{\xi+a}{a} & (0 < h < \infty) \\[2mm] -\tau\sqrt{x} & (h = \infty) \end{cases}$$

$$y_c(h,x,0,0,\tau) = \begin{cases} -\tau \dfrac{h}{2\pi a} \ln \dfrac{\xi+a}{a} & (0 < h < \infty) \\[2mm] +\tau\sqrt{x} & (h = \infty) \end{cases}$$

where ξ is defined by equation [2]. The effect of depth on $C_D(h,0,0,\tau)$

is shown in Figure 7(b). The upper and lower cavity shapes due to τ, for a number of depth-chord ratios, are shown in Figure 10.

THE INVERSE PROBLEM

To find the characteristics of a supercavitating hydrofoil of given shape, using the methods outlined herein, it is necessary to express the pressure distribution - or $\overline{u}(\xi)$ - in terms of the shape before the expressions (equations [11], [12], and [16]) for the lift, moment and drag coefficients can be used. The inversion of the integral equation in [15] was shown by Munk (7) to be

$$\overline{u}(\xi) = - \frac{\sqrt{1-\xi}}{\pi \sqrt{\xi}} \int_0^1 \frac{\sqrt{\xi'}\ \overline{v}\ (\xi')}{\sqrt{1-\xi'}\ (\xi - \xi')}\ d\xi', \quad 0 \leqslant \xi \leqslant 1 \qquad [31]$$

in which $\overline{v}(\xi')$ can be found from the shape by using equation [13].

Unfortunately the integrations involved in these operations when the hydrofoil is operating at a finite depth are, for all but the very simplest shapes, too complicated to be done analytically and would have to be done by numerical methods. At present, only the flat plate problem will be solved for finite depths. The problem of a flat plate with flap near a free surface has been dealt with elsewhere (14) and for very close approximations to the performance characteristics of two-, three-, and five-term and circular arc foils which are designed for infinite depth but operating at some other depth, the reader is referred to Johnson's work (6).

The Flat Plate at Finite Depths

The slope of a flat plate at an angle of attack δ to the direction of the flow is

$$\frac{dy_o}{dx} = - \delta\ .$$

We use equations [13] and [31] to obtain

$$\overline{u}(\xi) = \frac{\delta \sqrt{1-\xi}}{\pi \sqrt{\xi}} \int_0^1 \frac{\sqrt{\xi'} \, d\xi'}{\sqrt{1-\xi'} \, (\xi-\xi')} = - \delta \frac{\sqrt{1-\xi}}{\sqrt{\xi}} \qquad [32]$$

and combine this result with equations [11], [16] and [19] to get, for a flat plate,

$$C_L(h,0,\delta) = \begin{cases} \delta\pi & (h = 0 \\ \delta \frac{h}{a} \left(\sqrt{1+a} - \sqrt{a}\right)^2 & (0 < h < \infty) \\ \delta \frac{\pi}{2} & (h = \infty) \end{cases}$$

$$C_D(h,0,\delta,0) = \begin{cases} \pi\delta^2 & (h = 0) \\ \delta^2 \frac{h}{a} \left(\sqrt{1+a} - \sqrt{a}\right)^2 & (0 < h < \infty) \\ \frac{\pi}{2} \delta^2 & (h = \infty) \end{cases}$$

$$y_c(h,x,0,\delta,0) = \begin{cases} \delta \frac{h}{\pi} \left[\left(1+\frac{1}{2a}\right) \overline{P} + \sqrt{\frac{1+a}{a}} \, \overline{Q} - \frac{1}{a}\sqrt{\xi^2-\xi} \right. \\ \qquad\qquad \left. - \frac{\pi}{h} x \right] & (0 < h < \infty) \\ \frac{1}{2} \delta \left[\left(1+2\sqrt{x}\right)\sqrt{x+\sqrt{x}} - 2x \right. \\ \qquad \left. + \frac{1}{2} \ln \left(1+ 2\sqrt{x} - 2\sqrt{x+\sqrt{x}}\right) \right] & (h = \infty) \end{cases}$$

where $\overline{P} = \ln \left(1 - 2\xi - 2\sqrt{\xi^2-\xi}\right)$

$\overline{Q} = \ln \left(1 - \frac{2a+1}{a} \xi + 2\sqrt{\frac{a+1}{a}} \sqrt{\xi^2-\xi}\right) - \ln \frac{\xi+a}{a}$

and ξ is defined by equation [2].

HYDRONAUTICS, Incorporated

The variation of $C_L(h,0,\delta)$ and $C_D(h,0,\delta,0)$ and $C_M(h,0,\delta)$ with depth is shown in Figures 7(a) and 7(b). The moment coefficients were calculated by combining equations [32] and [11] and performing a numerical integration. The result is shown in Figure 7(c) as a plot of location of the center of pressure $(\dfrac{C_M}{C_L})$ on the hydrofoil vs. depth-chord ratio. The top cavity shape due to angle of attack for a number of depth-chord ratios is shown in Figure 11.

OPTIMUM FOILS AND FOIL STRENGTH

In accordance with equations [21], [23], [24], and [25] the lift, drag and upper and lower cavity ordinates of a foil in which camber, angle of attack and quasi-parobolic thickness are combined are found as follows:

$$C_L(h,k_1,\delta) = C_L(h,k_1,0,) + C_L(h,0,\delta)$$

$$C_D(h,k_1,\delta,\tau) = \left(\sqrt{C_D(h,k_1,0,0)} + \sqrt{C_D(h,0,\delta,0)} + \sqrt{C_D(h,0,0,\tau)}\right)^2$$

$$C_M(h,k_1,\delta) = C_M(h,k_1,0) + C_M(h,0,\delta)$$

$$y_0(h,x,k_1,\delta,\tau) = y_0(h,x,k_1,0,0)+y_0(h,x,0,\delta,0)+y_0(h,x,0,0,\tau)$$

$$y_c(h,x,k_1,\delta,\tau) = y_c(h,x,k_1,0,0)+y_c(h,x,0,\delta,0)+y_c(h,x,0,0,\tau)$$

Of the four camber configurations considered here it is clear that for given values of δ and τ, foils incorporating the five-term camber produce the highest lift-drag ratios. This conclusion is no longer significant, however, when the strength of

HYDRONAUTICS, Incorporated

-29-

these supercavitating hydrofoils is taken into consideration. For
purposes of strength calculations it is assumed that the foil sec-
tion is constructed so as to fill the entire thickness of the
cavity*, thus setting the foil thickness at any point along the
chord equal to $y_c(h,x,k_1,\delta,\tau) - y_o(h,x,k_1,\delta,\tau)$. The foil strength
is evaluated by considering the non-dimensional section modulus $\overline{Z}$
of a beam whose cross section is the hydrofoil section $\Big[\overline{Z} = Z/(c)^3$
where $Z = $ (area moment of inertia)$\Big/$(the distance between the neutral
axis and the furthest fiber)$\Big]$. In these calculations it is assumed
that the neutral axis of the beam is parallel to the reference
line $(y = 0)$ of the foil. Since the section modulus is calculated
mainly for comparison purposes it is of little consequence that
the true neutral axis may be oriented somewhat differently and that,
in addition, it may not always be practical to make the foil quite
as thick as the cavity.

The integrations involved in calculating the section modulus
must, of necessity, be carried out numerically for each specific
foil (i.e., a foil composed of a given set of the parameters h, k_1,
δ and τ). These calculations were first carried out by hand for
the two-term foil at a depth of one chord, using Simpson's Rule
in the calculation of the section moduli. Subsequently, a high
speed digital computer at the David Taylor Model Basin was used to
calculate the operating characteristics and section moduli of two-
term, three-term, five-term, and constant pressure camber hydrofoils,
designed for depth-chord ratios of $1/4$, $1/2$, 1, 2, 5 and ∞. In
these calculations the computer was programmed to consider for each
depth (a) all possible combinations of k_1, δ, and τ, with k_1 taking

---

*The upper surface of the foil is, however, still considered to be
unwetted.

on 10 values between 0 and 0.6, δ taking on 13 values between 0 and 3 degrees, and τ taking on 9 values between 0 and 1%; and (b) all possible combinations of the constant pressure camber configurations with each of the two-, three-, and five-term camber configurations, with k_1 taking on the same values as in (a). A sample of the results of these calculations is shown in Figure 12, in which contours of constant δ, k_2 and $\bar{Z}$ for a single value of τ are plotted on a grid of lift-drag ratio vs. lift coefficient, for a two-term hydrofoil designed for a depth of one chord. A subsequent report (No. 001-7) containing all the significant results of this computer study will be published in the near future. In addition, the computer program contained an optimization procedure in which the previously stored list of all the foils that had been computed for a given depth was searched for the three best foils (i.e., those with highest L/D) whose section modulus and lift coefficient were within certain prescribed ranges.

The optimization procedure showed that it is not possible to single out one type of camber distribution as being the absolute optimum for all depths, lift coefficients and section moduli. It is possible, however, to make the following generalizations:

(a) The combinations of the constant pressure camber with two-, three-, and five-term camber configurations are to be recommended only at very low depth-chord ratios (h < 0.5). At depth-chord ratios of 0.5 or higher this type of foil is efficient only for unrealistically high section moduli ($\bar{Z} > 12 \times 10^{-4}$) and unrealistically high lift coefficients ($C_L > .60$).

(b) Turning now to foils in which one of the four camber types is combined with angle of attack and quasi-parabolic thickness, it appears that except at unrealistically low section moduli ($\bar{Z} < 2 \times 10^{-4}$) the constant pressure and two-term are more efficient

than the three- and five-term camber configurations. This trend intensifies as either the section modulus or the design depth is increased, until, at infinite depth and high section moduli $(\overline{Z} > 6 \times 10^{-4})$ the constant pressure type of camber (combined with δ and τ) dominates the list of optimum foils.

In summary, the optimization process indicates that for practical values of depth-chord ratio, section modulus and lift coefficient (i.e., $h \geq 0.5$, $2 \times 10^{-4} \leq \overline{Z} \leq 6 \times 10^{-4}$ and $0.05 \leq C_L \leq 0.5$) the constant pressure and two-term camber configurations, each properly combined with angle of attack and quasi-parabolic thickness, deliver higher lift-drag ratios than the other types of camber. The two-term foils are, usually, the better of these two and in cases in which the constant pressure camber is somewhat superior the difference between its lift-drag ratio and that of the two-term foils is not very significant.

In Figure 13 a typical, two-dimensional, two-term hydrofoil is drawn to scale. This particular foil is designed for operation at a depth of one chord and is composed of camber index $k_2 = 0.15$, design angle of attack $\delta = 1.6^\circ$ and quasi-parabolic thickness $\tau = 0.004$. It develops a lift coefficient of 0.195 and a lift-cavity drag ratio of 34.5 and its nominal section modulus is $\overline{Z} = 4.1 \times 10^{-4}$.

HYDRONAUTICS, Incorporated

REFERENCES

1. A. E. Green, "Note on the Gliding of a Plate on the Surface of a Stream", Proc. Cambridge Phil. Soc., Vol. XXXII, Pt. 2, May 1936, pp. 248-252.

2. V. E. Johnson, Jr., "Theoretical and Experimental Investigation of Arbitrary Aspect Ratio, Supercavitating Hydrofoils Operating Near the Free Water Surface", NACA RM L57I16, December 1957.

3. M. P. Tulin and M. P. Burkart, "Linearized Theory for Flows About Lifting Foils at Zero Cavitation Number", DTMB Report C-638, February 1955.

4. Virgil E. Johnson, Jr., "Theoretical Determination of Low-Drag Supercavitating Hydrofoils and Their Two-Dimensional Characteristics at Zero Cavitation Number", NACA RM L57G11a, September 1957.

5. A. J. Tachmindji, W. B. Morgan, M. L. Miller, and R. Hecker, "The Design and Performance of Supercavitating Propellers", DTMB Report C-807, February 1957.

6. V. E. Johnson, Jr., "The Influence of Submersion, Aspect Ratio and Thickness on Supercavitating Hydrofoils Operating at Zero Cavitation Number", Presented at the Second Symposium on Naval Hydrodynamics, Washington, D. C., August 1958.

7. M. M. Munk, "Elements of the Wing Section Theory and of the Wing Theory", NACA Report No. 191, 1924.

8. H. Wagner, "Über das Gleiten von Wasserfahrzeugen", Jahrbuch der Schiffbautechnik, v. 34, 1933. Also published in English as "Planing of Watercraft", NACA TM 1139, April 1948.

9. R. T. Jones and D. Cohen, "High Speed Wing Theory", Princeton University Press, 1960.

10. W. Gröbner and N. Hofreiter, "Integraltafel", vol. I and II, Springer Verlag, Wien and Innsbruck, 1958.

11. M. P. Tulin, "Steady Two-Dimensional Cavity Flows About Slender Bodies", Appendix 1, DTMB Report 834, May 1953.

HYDRONAUTICS, Incorporated

12. Bryan Thwaites (editor), "Incompressible Aerodynamics", Chapter IV, p. 23, Fluid Motion Memoirs, Oxford at the Clarendon Press, 1960.

13. G. H. Peebles, "A Method for Calculating Airfoil Sections from Specifications on the Pressure Distributions", Journal of the Aeronautical Sciences, V. 14, No. 8, August 1947.

14. J. Auslaender, "The Behavior of Supercavitating Foils with Flaps Operating at High Speed Near a Free Surface", HYDRONAUTICS, Incorporated, Technical Report 001-2, July 1960.
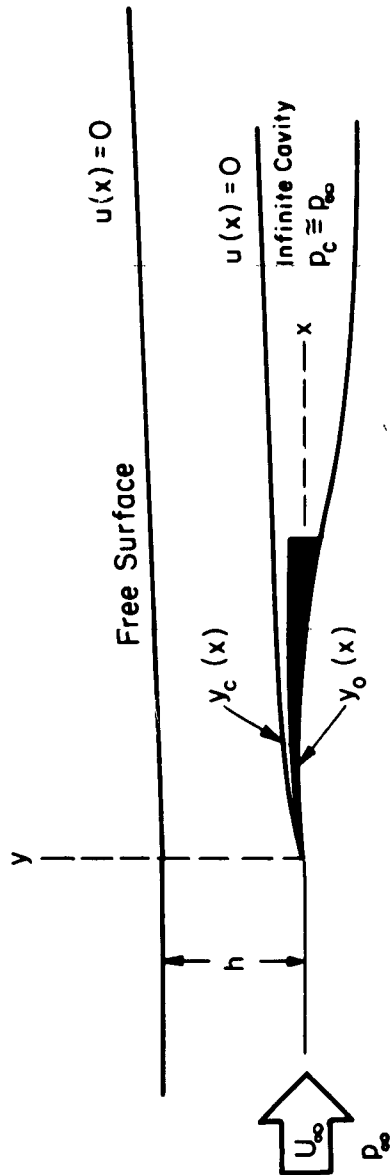
Figure 1 – Supercavitating or Ventilated Flow near a Free Surface at $\sigma \cong 0$

Hydrofoil Plane $(z = x + iy)$

$$\frac{dz}{d\zeta} = \frac{A\,\zeta}{\zeta + a}$$

Airfoil Plane $(\zeta = \xi + i\eta)$
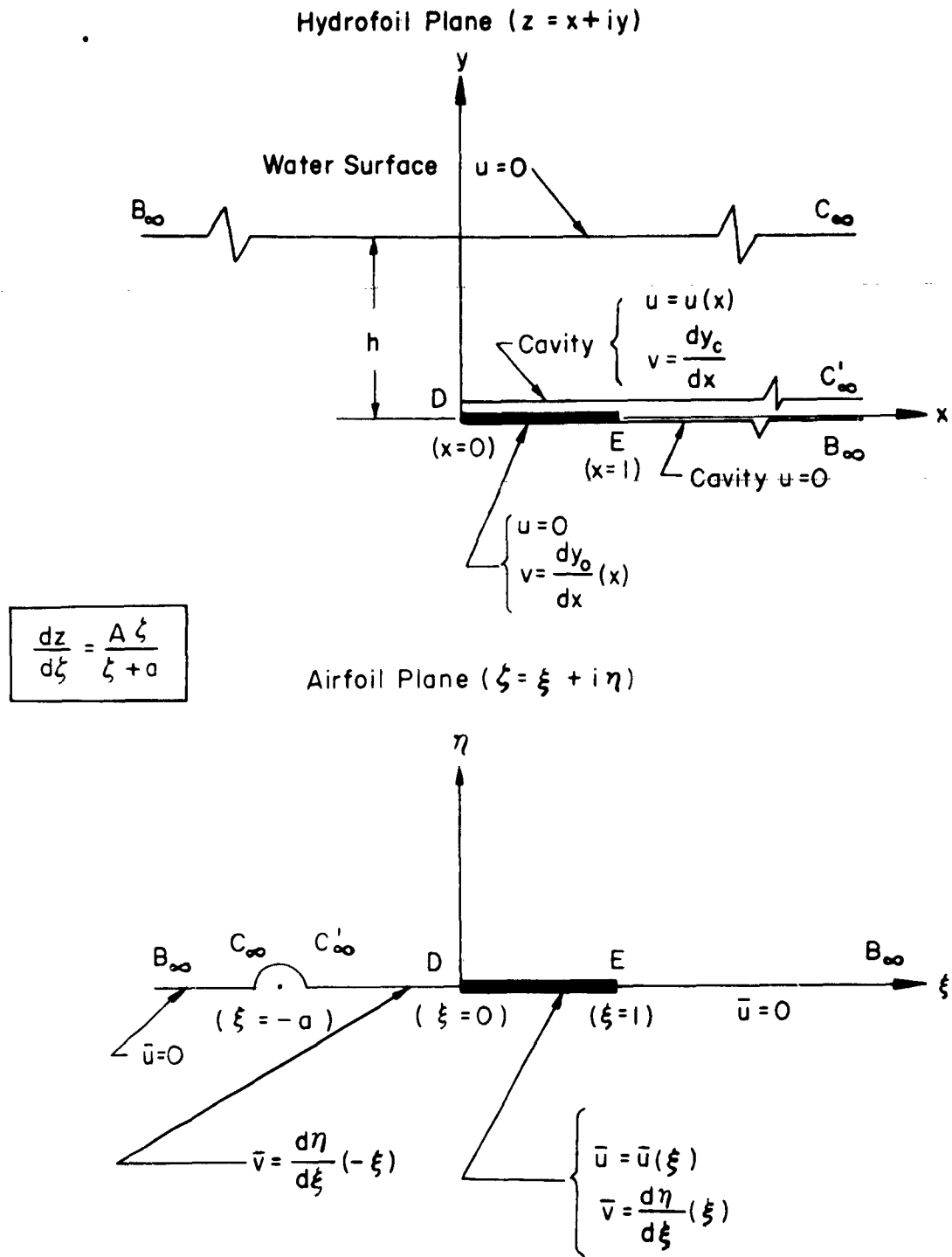
Figure 2 — The Linearized Version of a Supercavitating Hydrofoil near a Free Surface Transformed into its Equivalent Airfoil; $\sigma = 0$
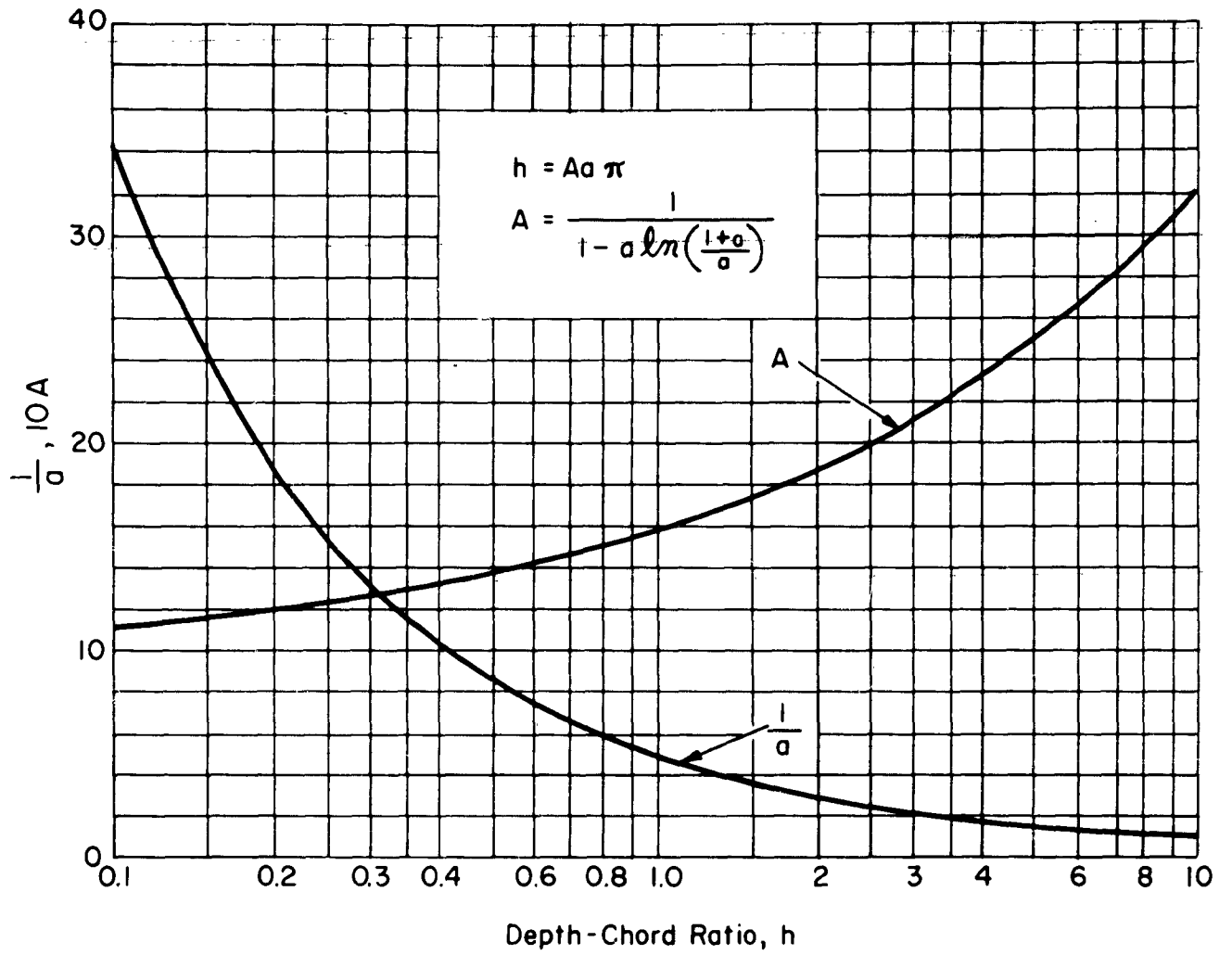
Figure   3 - Transformation Parameters
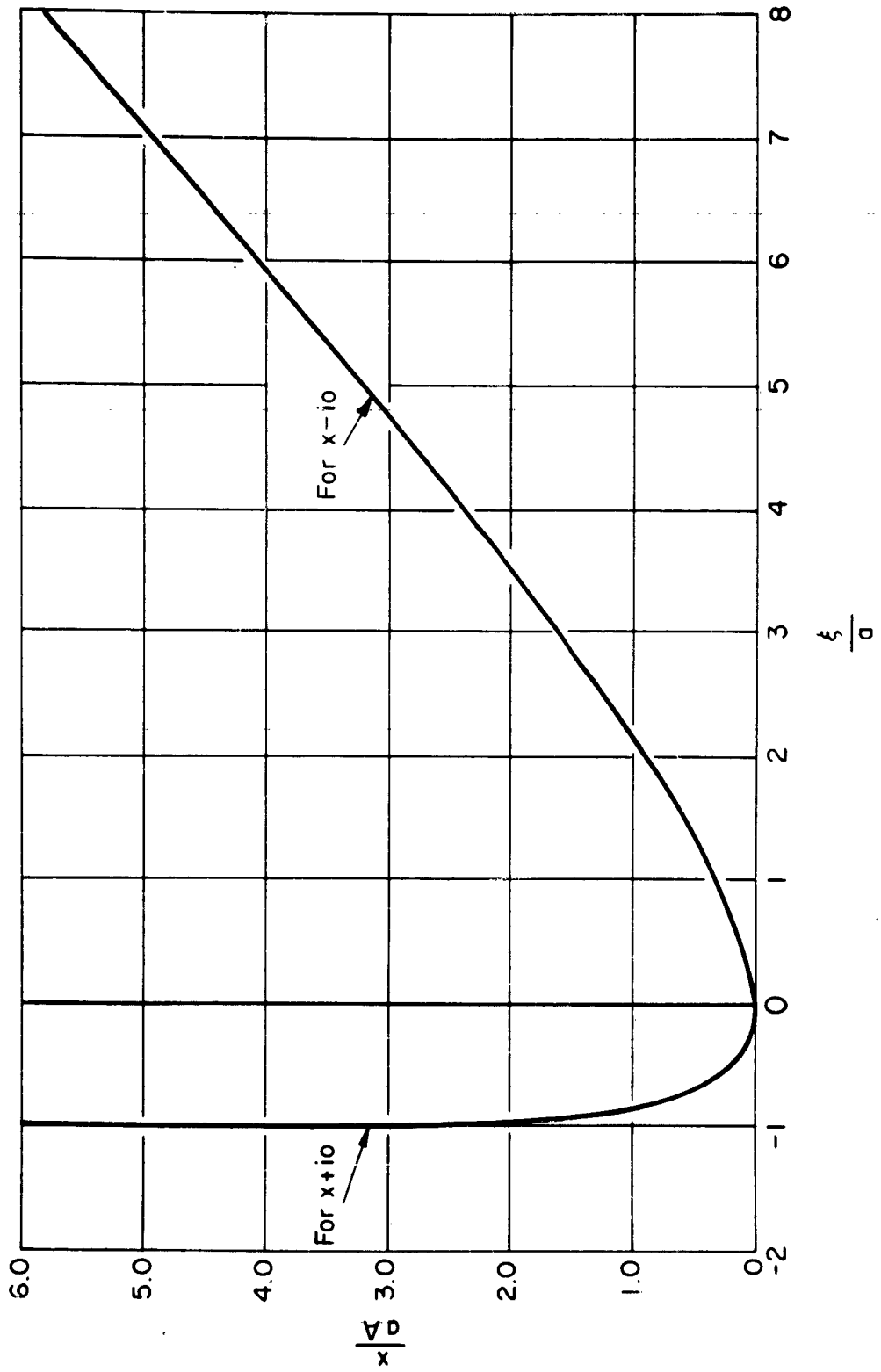
Figure 4 — The $x - \xi$ Transformation
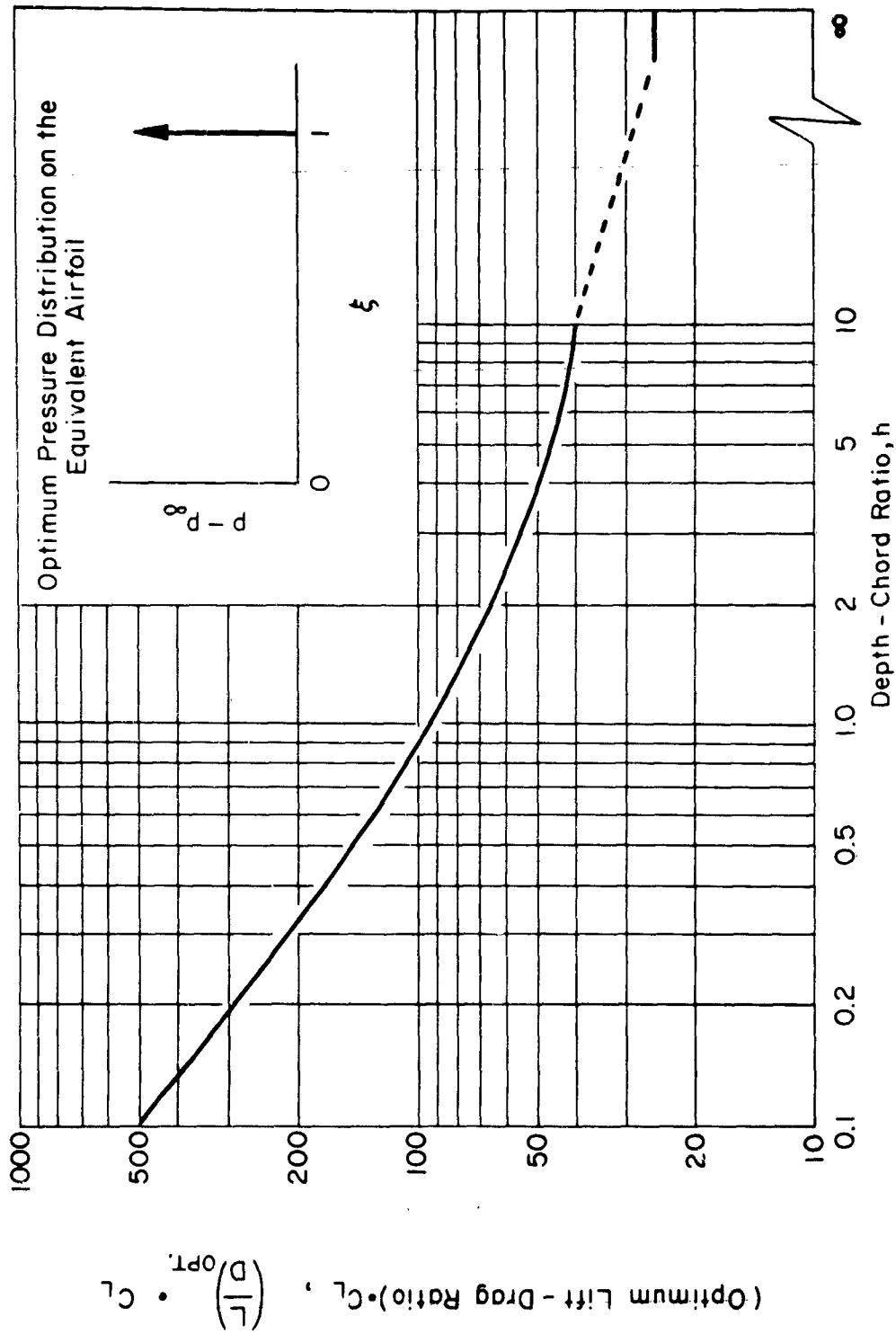
Figure 5 — Variation of the Optimum Lift-Drag Ratio with Depth
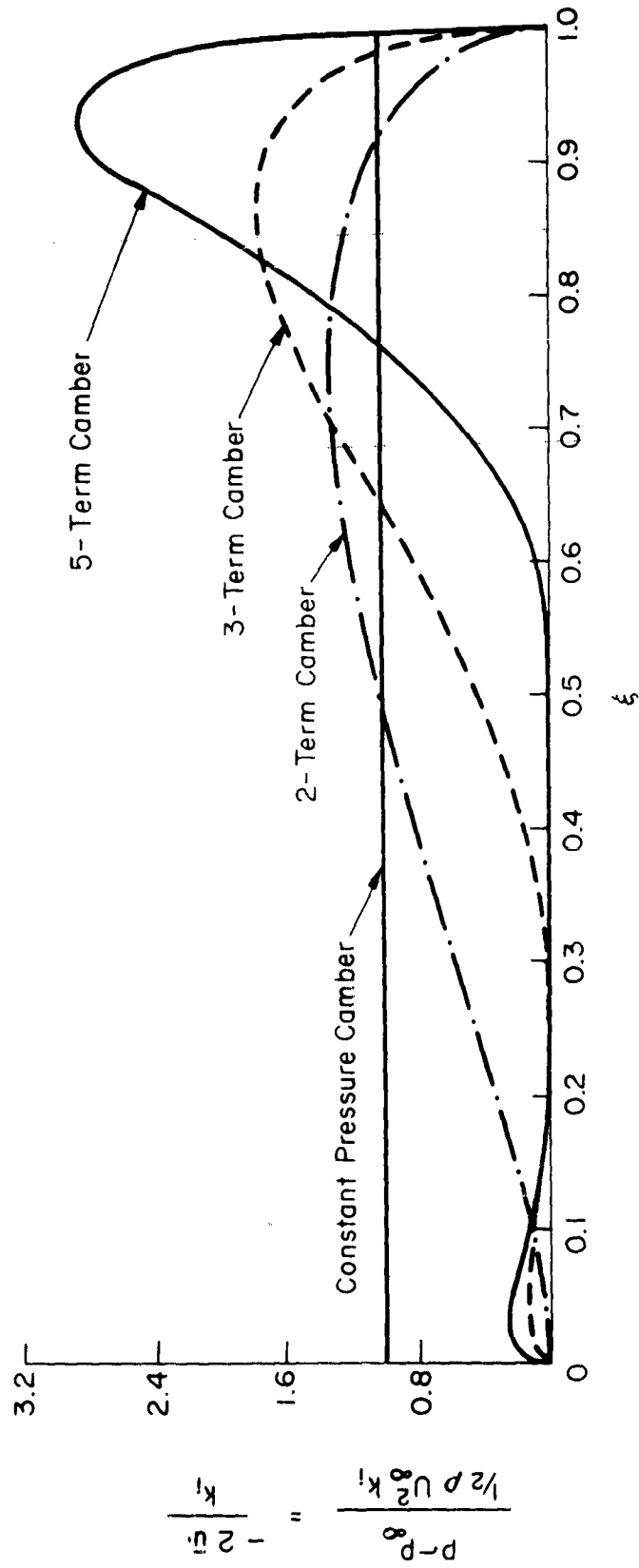
Figure 6 – Pressure Distribution on the Bottom of the Equivalent Airfoil for Four Types of Camber Distribution

$$\frac{p - p_\infty}{\frac{1}{2}\rho U_\infty^2 k_i} = \frac{-2\bar{u}_i}{k_i}$$
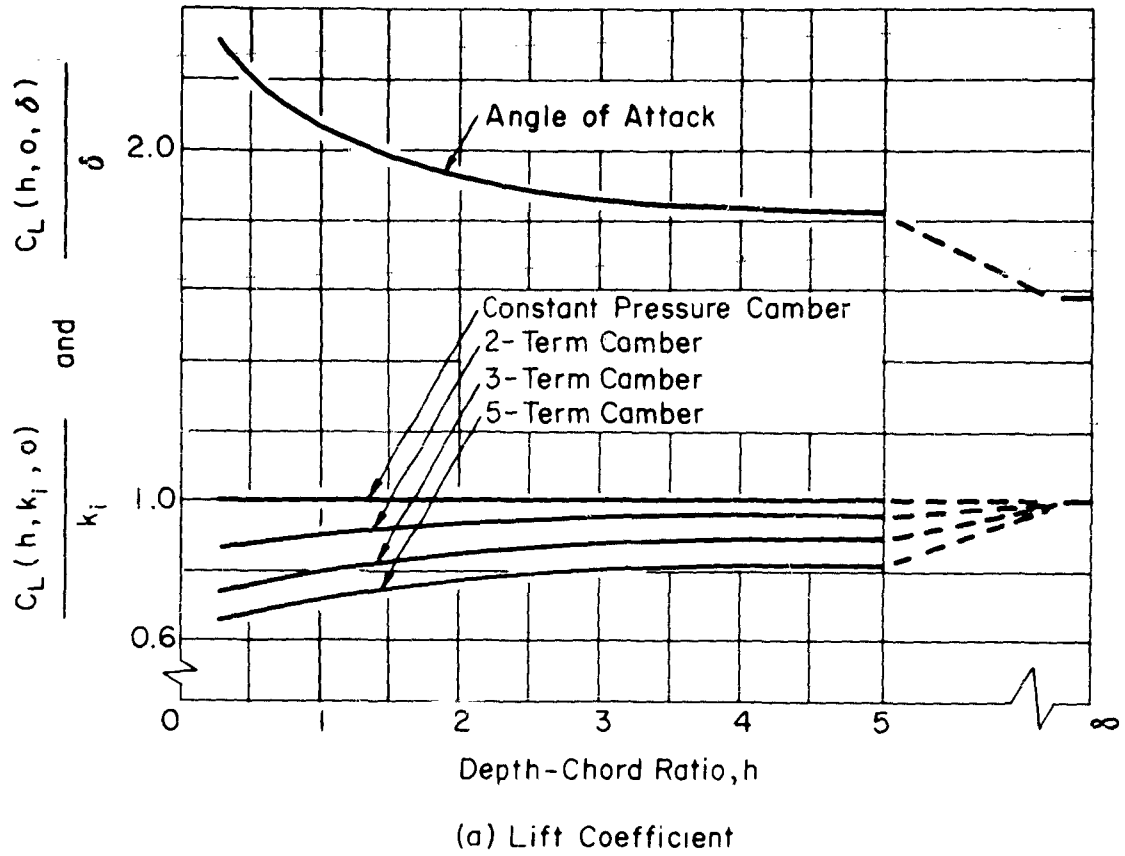
(a) Lift Coefficient

Figure 7 – The Influence of Depth on Lift Coefficient, Drag Coefficient
and Location of the Center of Pressure due to Camber, Angle
of Attack and Quasi-Parabolic Thickness
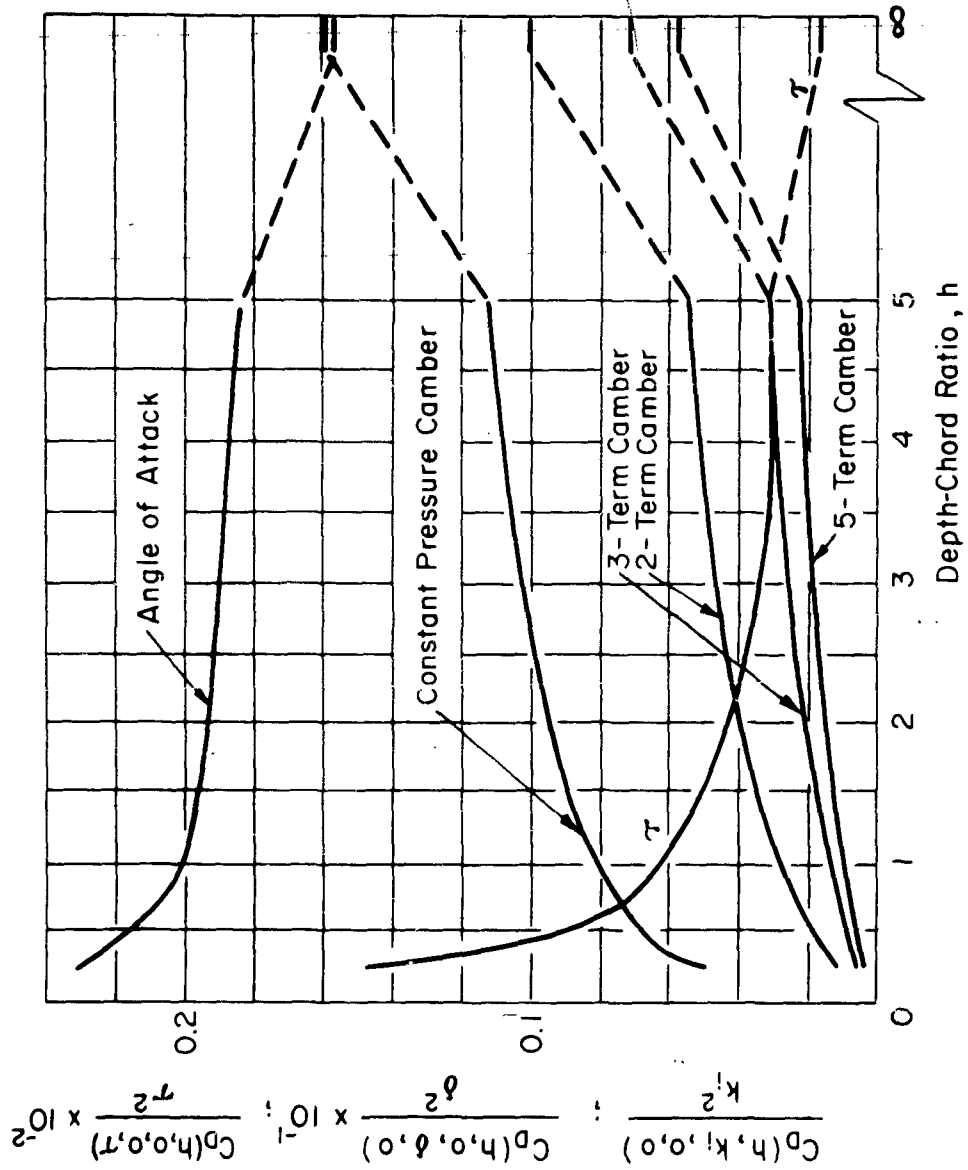
Figure 7 – (Continued)

(b) Drag Coefficient
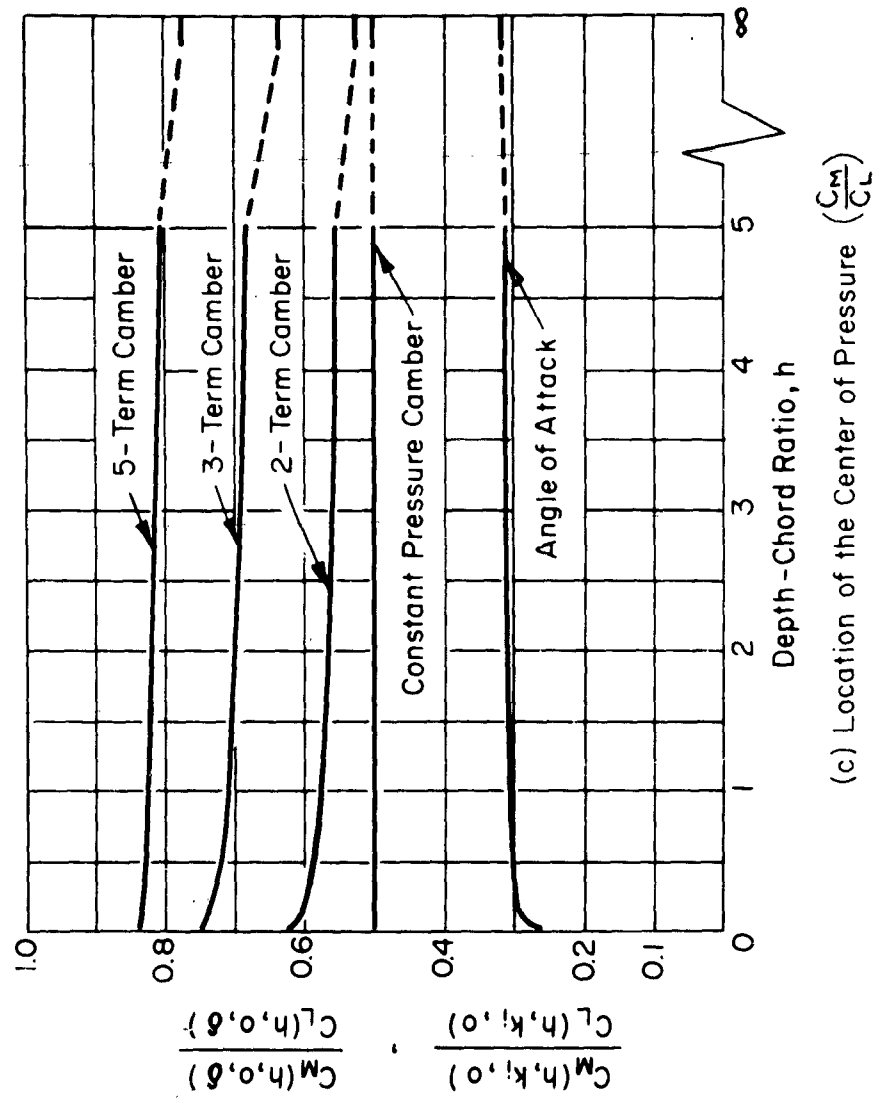
(c) Location of the Center of Pressure $\left(\dfrac{C_M}{C_L}\right)$

Figure 7 – (Concluded)
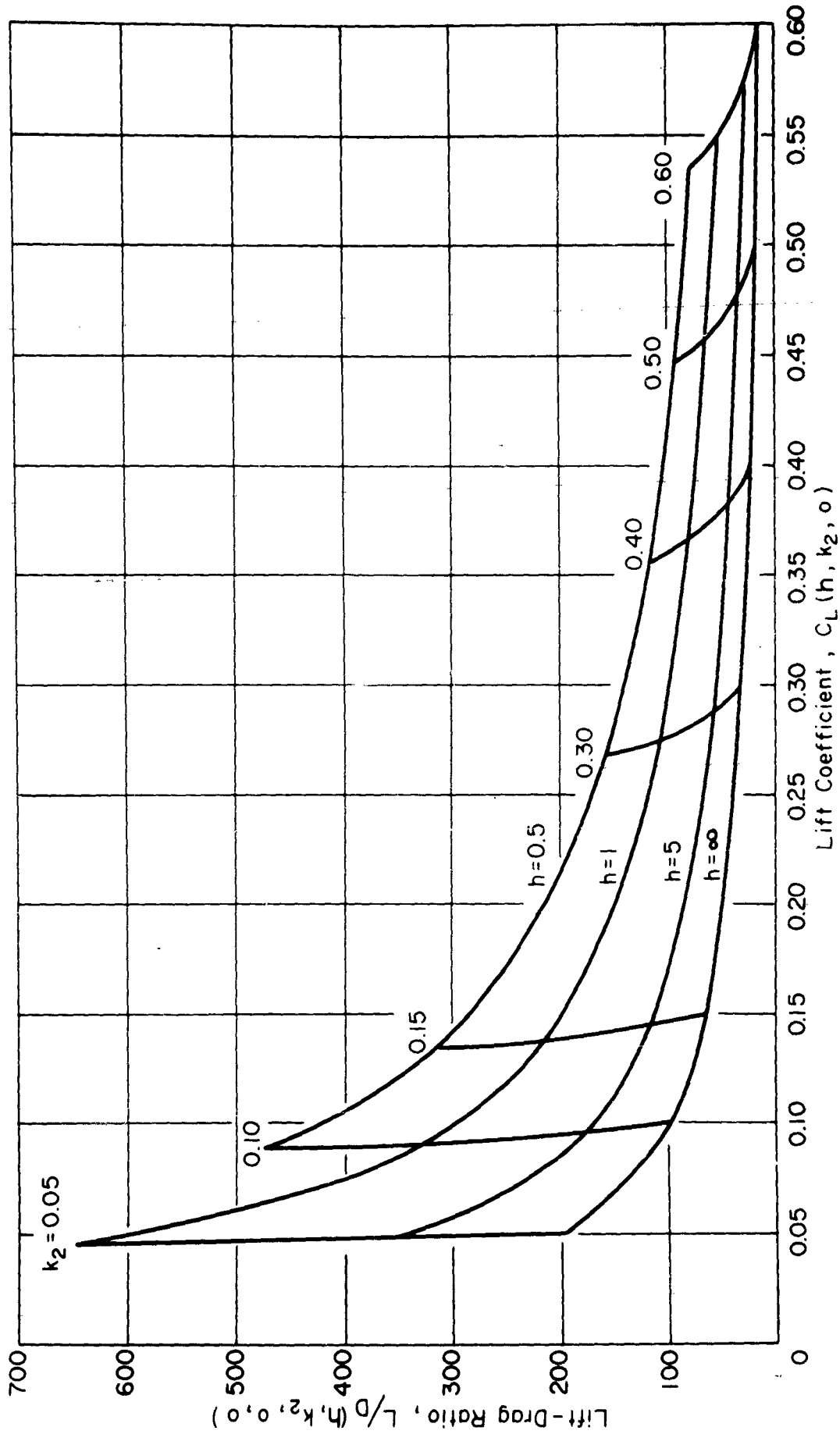
Figure 8 — Lift-Drag Ratio of the Two-Term Camber without Angle of Attack and Quasi-Parabolic Thickness

Figure 9— Bottom Surface, y_o, and Top Cavity Boundary, y_c, of Four Camber
Configuration Designed for Specific Depths
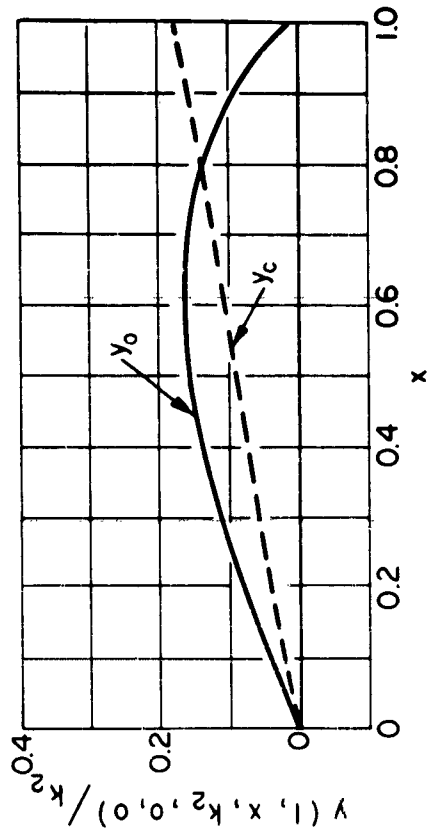
(a)-One Chord Depth
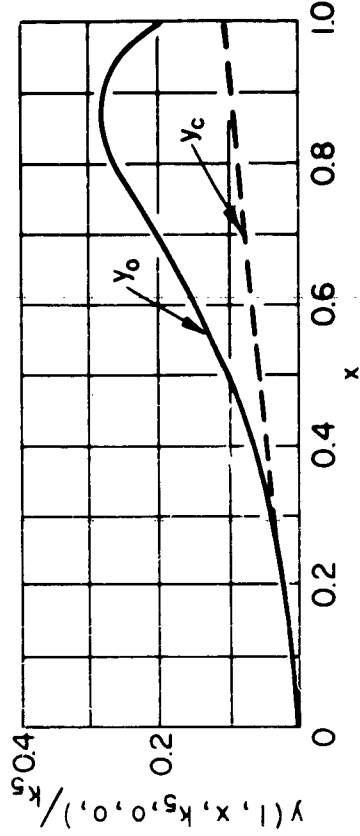
Two-Term Camber

Five-Term Camber
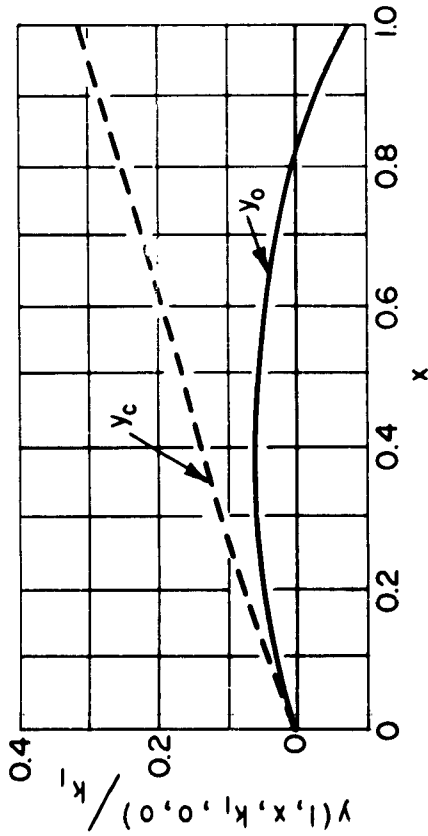
Constant Pressure Camber

Three-Term Camber
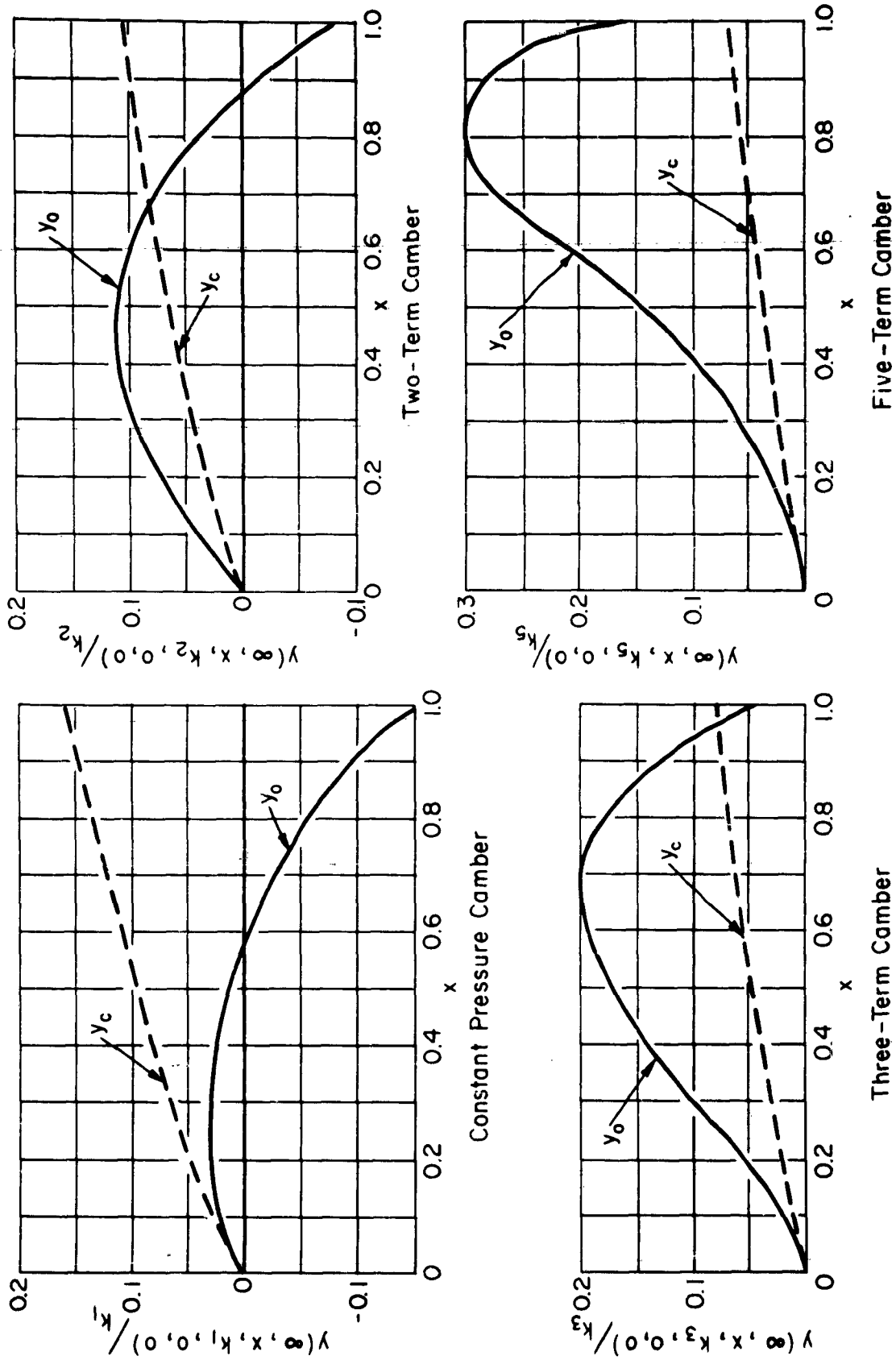
(b)- Infinite Depth

Figure 9 — Concluded
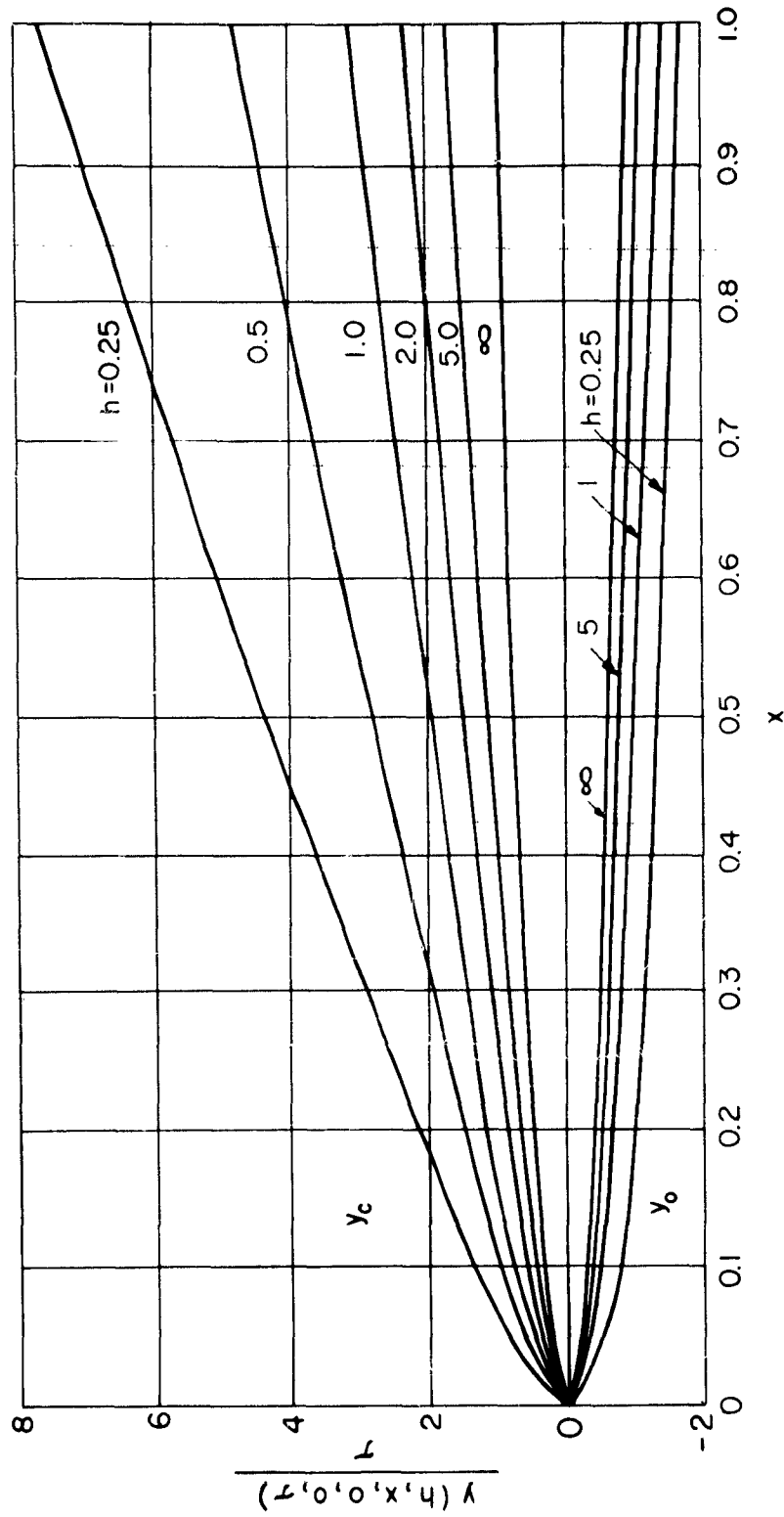
Figure 10 - Bottom Surface, y_o, and Top Cavity Boundary, y_c, of Quasi-Parabolic Thickness, at Various Depths of Submersion
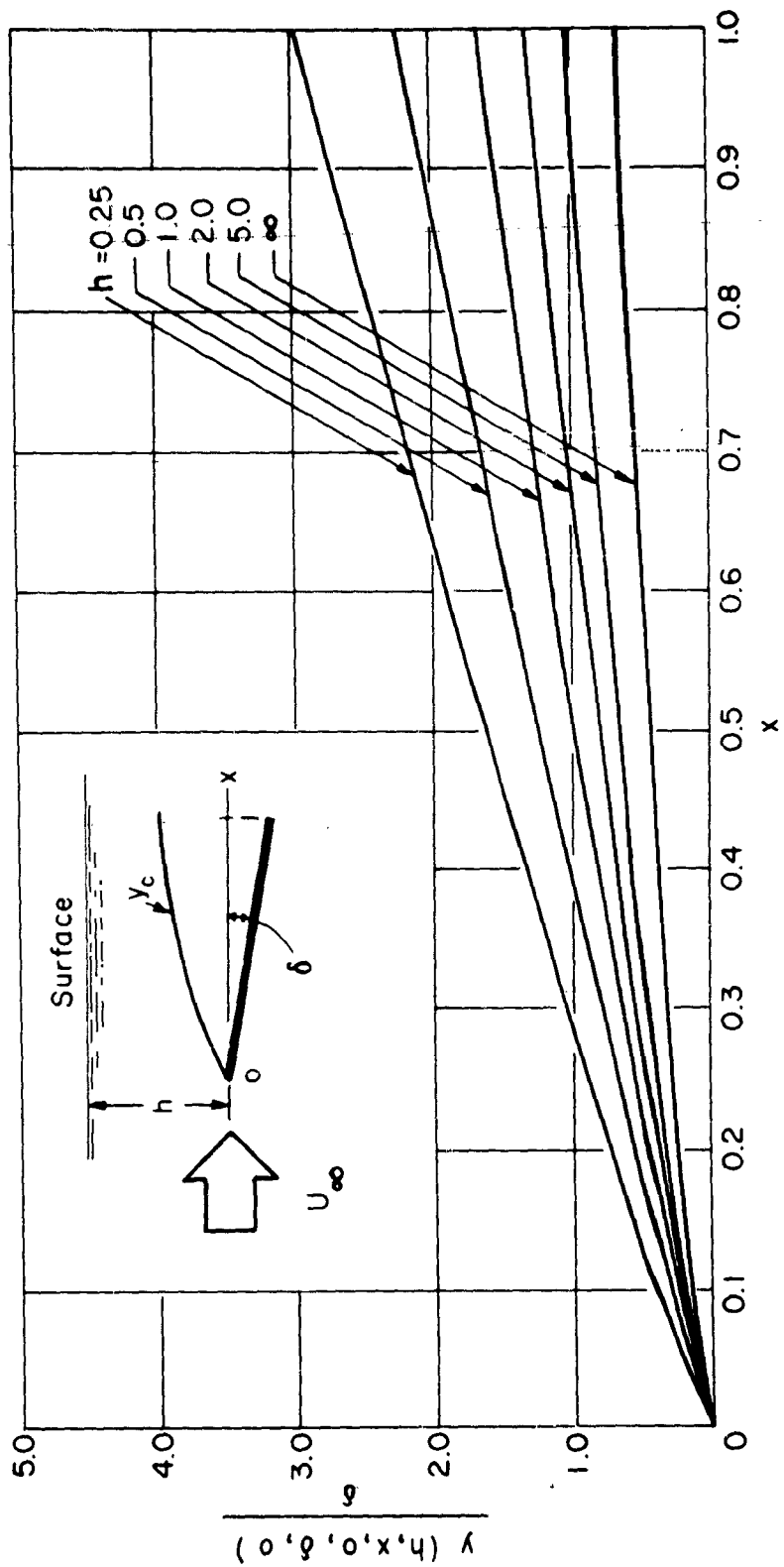
Figure II — Top Cavity Boundary due to an Inclined Flat Plate at Various Depths
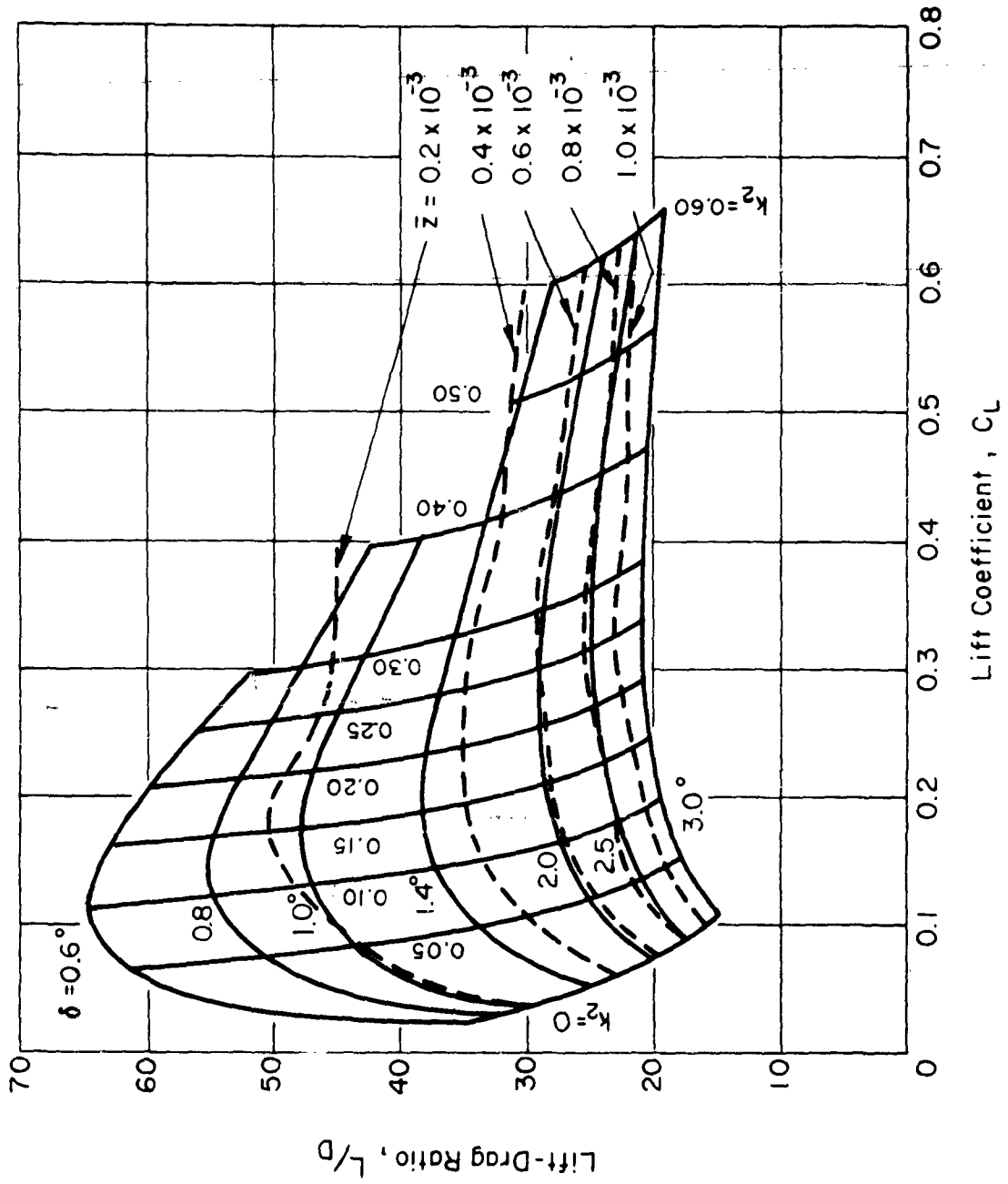
Figure   12 – Lift-Drag Ratio versus Lift Coefficient of a Two-Term Foil with Angle of Attack and Quasi-Parabolic Thickness, $\tau = 0.004$; $h = 1$

Enlarged Leading Edge

$k_2 = 0.15$
$\delta = 1.6°$
$\tau = 0.004$
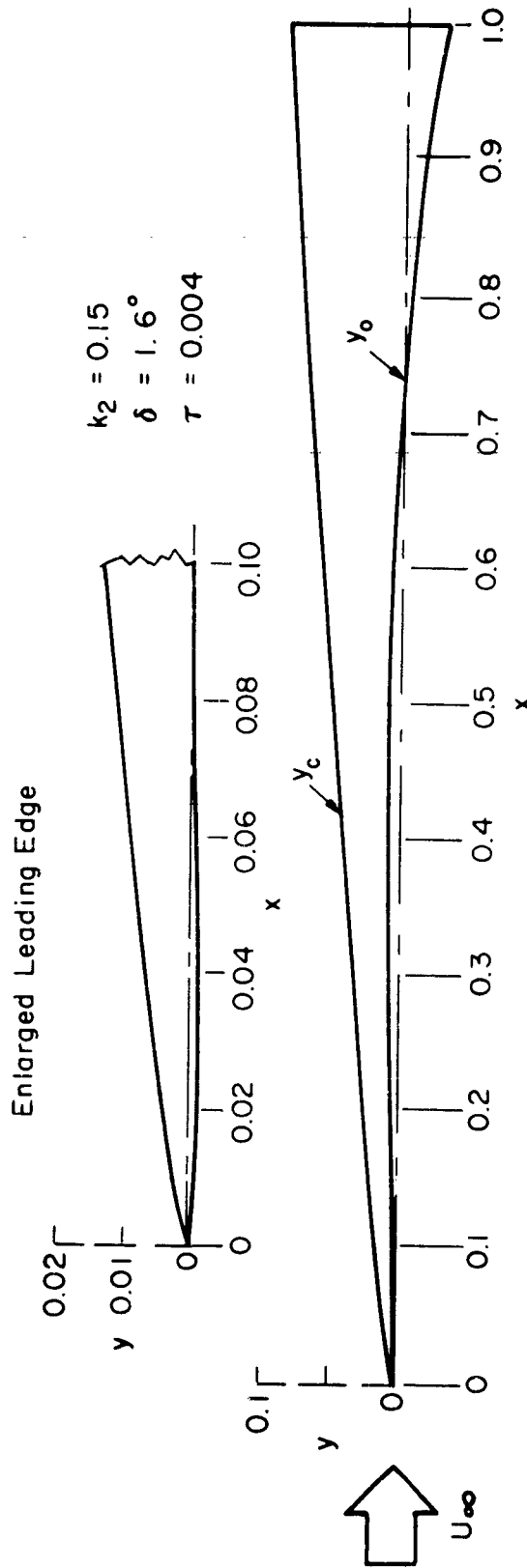
Figure 13 – Typical Two-Dimensional, Two-Term Hydrofoil Designed for Operation at a Depth of One Chord ; $C_L = 0.195$; $L/D = 34.5$; $\bar{z} = 0.410 \times 10^{3}$

HYDRONAUTICS, Incorporated

DISTRIBUTION LIST

BuShips Contract NObs-78396

Number of Copies

Chief, Bureau of Ships (60)
Navy Department
Washington 25, D. C.
ATTN: Code 106   1
       Code 335   3
       Code 410   1
       Code 420   53
   Code 442   1
       Code 449   1

Chief, Office of Naval Research (2)
Navy Department
Washington 25, D. C.
ATTN: Code 438   2

Commanding Officer and Director (6)
David Taylor Model Basin
Carderock, Maryland
ATTN: Code 500   1
       Code 513   1
       Code 520   1
       Code 526   1
       Code 530   1
       Code 580   1

Chief, Bureau of Naval Weapons (2)
Navy Department
Washington 25, D. C.
ATTN: Code RAAD-343   1
       Code R-52   1

Commander
Armed Services Technical Information Agency
Arlington Hall Station
Arlington 12, Virginia
ATTN: TIPDR   5

(1)

HYDRONAUTICS, Incorporated

Mr. John B. Parkinson
Langley Aeronautical Laboratory
National Aeronautics and Space Administration
Langley Field, Virginia   1

Boeing Airplane Company
Aero-Space Division
Box 3707
Seattle 24, Washington   1

California Institute of Technology
Pasadena, California
ATTN: Professor T. Y. Wu
        Hydrodynamics Laboratory   1

Convair Hydrodynamic Laboratory
Convair Division
General Dynamics Corporation
San Diego, California   1

Director, Stevens Institute of Technology
Davidson Laboratory
Castle Point Station
Hoboken, New Jersey   1

Grumman Aircraft Engineering Corporation
Marine Engineering Section
Bethpage, Long Island, New York   1

Hughes Aircraft Company
Systems Development Laboratories
Culver City, California
ATTN: Mr. W. N. Turner   1

Hydronautics, Incorporated
200 Monroe Street
Rockville, Maryland   1

The Martin Company
Baltimore 3, Maryland
ATTN: Mr. John D. Pierson   1

(2)

HYDRONAUTICS, Incorporated

Massachusetts Institute of Technology
Department of Naval Architecture and
    Marine Engineering
Cambridge 39, Massachusetts   1

Director
University of Minnesota
St. Anthony Falls Hydraulic Laboratory
Hennepin Island
Minneapolis 14, Minnesota   1

Southwest Research Institute
Department of Applied Mechanics
8500 Culebra Road
San Antonio 6, Texas   1

Technical Research Group, Inc.
2 Aerial Way
Syosset, New York   1

Chief of Naval Operations
Navy Department
Washington 25, D. C.
ATTN: Capt. N. H. Fisher, OP-712   1